HHS Public Access

Author manuscript

Dev Cell. Author manuscript; available in PMC 2020 May 20.

Published in final edited form as:

Dev Cell. 2019 May 20; 49(4): 574–589.e5. doi:10.1016/j.devcel.2019.03.029.

An SH3PX1-dependent endocytosis/autophagy network restrains intestinal stem cell proliferation by counteracting EGFR/ERK signaling

Peng Zhang[1], **Andreana N. Holowatyj**[2], **Taylor Roy**[1], **Stephen M. Pronovost**[1], **Marco Marchetti**[1], **Hanbin Liu**[1], **Cornelia M. Ulrich**[2,3], and **Bruce A. Edgar**[1,4,※]

[1]Huntsman Cancer Institute and Department of Oncological Sciences, University of Utah, Salt Lake City, UT 84112, USA

[2]Huntsman Cancer Institute and Department of Population Health Sciences, University of Utah, Salt Lake City, UT 84112, USA

[3]Fred Hutchinson Cancer Research Center, Seattle, WA 98109, USA

[4]Lead contact

SUMMARY

The effect of intracellular vesicle trafficking on stem cell behavior is largely unexplored. We screened the *Drosophila* sorting nexins (SNXs) and discovered that one, SH3PX1, profoundly affects gut homeostasis and lifespan. SH3PX1 restrains intestinal stem cell (ISC) division through an endocytosis/autophagy network that includes Dynamin, Rab5, Rab7, Atg1, 5, 6, 7, 8a, 9, 12, 16, and Syx17. Blockages in this network stabilize ligand-activated EGFRs, recycling them via Rab11-dependent endosomes to the plasma membrane. This hyperactivated ERK, calcium signaling, and ER stress, autonomously stimulating ISC proliferation. The excess divisions induced epithelial stress, Yki activity, and Upd3 and Rhomboid production in enterocytes, catalyzing feed-forward ISC hyperplasia. Similarly, blocking autophagy increased ERK activity in human cells. Many endocytosis/autophagy genes are mutated in cancers, most notably those enriched in microsatellite instable-high and *KRAS*-wildtype colorectal cancers. Disruptions in endocytosis and autophagy may provide an alternative route to RAS/ERK activation, resulting in EGFR-dependent cancers.

Graphical Abstract

※ Correspondence: Bruce A. Edgar (bruce.edgar@hci.utah.edu).

AUTHOR CONTRIBUTIONS

Conceptualization was provided by P.Z. and B.A.E.; Methodology was designed by P.Z., A.N.H. and M.M.; Investigations were carried out by P.Z., T.R., S.M.P., A.N.H., M.M. and H.L.; Formal analyses were performed by P.Z., A.N.H. and M.M.; P.Z. wrote the manuscript with input from B.A.E., T.R., A.N.H. and S.M.P.; All authors reviewed the manuscript.

Declaration of Interests

The authors declare no competing interests.

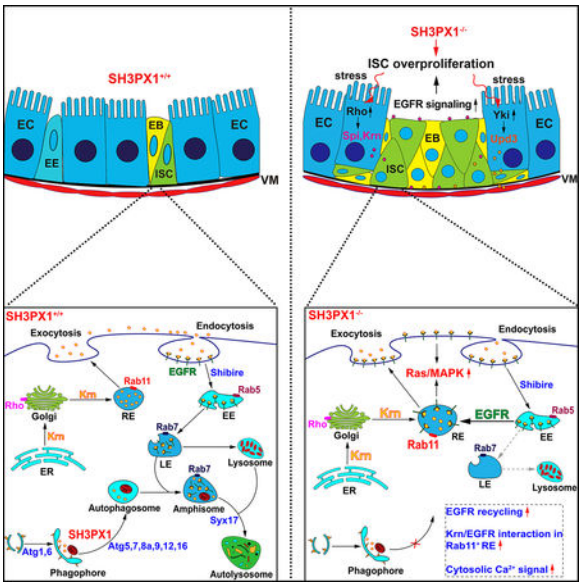

The origins and functions of resident immune cells in barrier tissue are highly diverse. Lin et al. identify in the zebrafish epidermis an ectoderm-derived immune cell type – metaphocytes – that capture soluble antigens from external environment through transepithelial protrusions and convey these antigens to conventional Langerhans cells via an apoptosis-phagocytosis pathway.

INTRODUCTION

In the intestine, genetic and epigenetic changes that dysregulate epithelial homeostasis contribute to common maladies such as colorectal cancer (CRC) and inflammatory bowel diseases (IBD) (Pesic and Greten, 2016). Cancer genetics suggests that many of the genes and pathways that affect gut epithelial homeostasis remain either unknown, or poorly characterized in the context of real epithelia. However, such genes can be readily identified and functionally analyzed in the gut epithelium of *Drosophila*, which shares many similarities with its human counterpart. Epithelial renewal in the fly's midgut is sustained by intestinal stem cells (ISCs) that divide to renew themselves and also produce transient cells (enteroblasts; EBs) that further differentiate into multiple types of enterocytes (ECs) or enteroendocrine (EE) cells (Micchelli and Perrimon, 2006; Ohlstein and Spradling, 2006). The intestinal epithelium turns over rapidly in both humans and insects, at rates that vary from days to weeks according to food composition, ingested toxins and pathogens (Jiang et al., 2009; Ohlstein and Spradling, 2006). Under both normal homeostatic and stressed conditions, ISC divisions are regulated by numerous signaling pathways that maintain the critical balance between cell generation and loss (Jiang and Edgar, 2011; Miguel-Aliaga et al., 2018). But how the cell biology of ISCs impacts signal transduction in these pathways and maintains the critical signaling balance necessary for epithelial homeostasis, remains largely unexplored.

Recent studies show that calcium signaling integrates diverse mitogenic signaling inputs that control ISC proliferation (Deng et al., 2015; Xu et al., 2017), and accumulating evidence indicates that calcium fluxes are involved in many constitutive membrane trafficking events

(Hay, 2007). However, whether intracellular vesicle trafficking affects ISC division and gut homeostasis has not been checked. One family of genes that regulate intracellular membrane traffic are the sorting nexins (SNXs), evolutionarily conserved proteins that are classified by the presence of phox-homology (PX) domains (Cullen, 2008). The phosphoinositide-binding ability of the PX domain explains in part the role for SNX in multiple steps of membrane trafficking including endocytosis, endosomal sorting and signaling. Not surprisingly, *SNX* mutations have increasingly been associated with diseases (*e.g.*, Alzheimer's disease and various cancers) in which endosomal function is compromised (Teasdale and Collins, 2012). The human genome encodes 33 known SNXs (Cullen, 2008) that can be classified on the basis of common domain structures into different subfamilies: PX-only, PX-BAR, SH3-PX-BAR and PX-FERM (Teasdale and Collins, 2012). Nine *Drosophila* SNXs are conserved with the 33 human SNXs (Rodal et al., 2011; Zhang et al., 2011), but little is known of their *in vivo* functions. SNX3, a PX-only subfamily member, is reportedly a component of the Retromer complex, which regulates Wnt/Wingless secretion (Zhang et al., 2011). SNX16 complexes with Nervous Wreck (Nwk) to control synaptic growth signaling (Rodal et al., 2011). The fly ortholog of human SNX9, 18, and 33, called SH3PX1, is required for autophagosome formation in the fat body (Knaevelsrud et al., 2013).

Over the past decade, autophagy has been linked to diverse pathophysiological processes including metabolic and neurodegenerative disorders, cardiovascular diseases and cancer (Levine and Kroemer, 2008). Yet while autophagy has been reported to affect stem cell maintenance and differentiation (Vessoni et al., 2012), the precise mechanisms underlying these consequences are unclear. Several studies report that autophagy genes are required in intestinal epithelial cells (iECs) for ISC maintenance and CRC formation, presumably via cell non-autonomous mechanisms. Asano *et al* showed that deletion of *Autophagy-related gene 5* (*ATG5*) in murine iECs using *Villin-Cre* (a pan-iEC recombinase), or in Paneth cells using *Ah-Cre*, led to a decrease in ISCs over time (Asano et al., 2017). Lévy *et al* showed that knockout of *ATG7* in iECs inhibits adenoma formation in $APC^{+/-}$ mice (Levy et al., 2015). Loss of function studies of *ATG16L1* show that this autophagy gene, which is associated with bowel inflammation in Crohn's disease, is necessary for Paneth cell survival and secretory function (Bel et al., 2017; Cadwell et al., 2008; Matsuzawa-Ishimoto et al., 2017). So far, however, the roles of autophagy and endosomal trafficking general have not been investigated specifically in ISCs using ISC-targeted deletions. Moreover, the effect of SNX-mediated endosomal trafficking on ISC functions is still unknown.

In this study, a screen of the entire family of *Drosophila* SNXs discovered that one, SH3PX1, is critical for restraining ISC proliferation and maintaining gut epithelial homeostasis. SH3PX1 accomplishes this via its role in an extended endocytosis/autophagy network that contains many other genes that similarly affect ISCs. Further, we found that EGFR/Ras/MAPK signaling is the primary trigger for ISC proliferation upon disruption of the endocytosis/autophagy network. Blocking autophagy and re-routing endosomal traffic in this network leads to accumulation of ligand-activated EGF receptors in Rab11-dependent endosomes, increased ERK and Ca^{2+} signaling, and ER stress in ISCs, thereby driving their division. We noted similar effects with autophagy inhibitors in human cells. In human cancers, SNX9, 18, and 33 and other endocytosis and autophagy genes are commonly altered. This occurs most significantly in CRC where these genes are tightly associated with

microsatellite instable-high (MSI-H) and CpG island methylator phenotype-high (CIMP-H) molecular phenotypes. A negative association was also uncovered between loss-of-function mutations in *SNX9/18/33* and activating *KRAS* mutations. This suggests, like our *Drosophila* work, that the disruption of the endocytosis/autophagy network provides an alternate route to EGFR signaling activation in human cancers. The endocytosis/autophagy network may offer new diagnostic and therapeutic strategies for CRC and other EGFR-dependent diseases that involve excessive stem cell proliferation and epithelial turnover.

RESULTS

Drosophila SH3PX1 restrains ISC proliferation

Nine sorting nexin genes (*Snx1*, *Snx3*, *Snx6*, *SH3PX1*, *Snx16*, *Snx17/CG5734*, *Snx21/CG3077*, *snz*, and *Snx27/CG32758*) have been identified in *Drosophila* (Rodal et al., 2011; Zhang et al., 2011). All of the *Snx* null mutants except *Snx17* were homozygous viable and had no obvious developmental defects (Rodal et al., 2011; Zhang et al., 2011), thereby allowing examination of ISC status in mutant adults. Three *SNXs* were shown to regulate ISC mitoses: *SH3PX1*, *SNX16* and *Snz*. *SNX16* mutants had a modest upregulation of ISC mitoses, whereas homozygous *Snz* mutants exhibited a mild repression of ISC mitoses relative to heterozygous controls (Figure 1A). Homozygous mutants of $SH3PX1^{d1/d1}$ (a P-element excision null allele, Figures S1A–S1B) showed a strong increase in ISC mitoses (Figure 1A). As evaluated using *miranda-GFP* (*mira-GFP*), a marker for ISCs and EBs (Bardin et al., 2010), homozygous $SH3PX1^{d1/d1}$ mutants had marked increases in GFP^{+} cells compared with heterozygote controls (Figure 1B). MARCM clonal analysis showed that the $SH3PX1^{d1/d1}$ mutant cells grew faster than controls, generating larger than normal clones after 14 days (Figures S3A–S3C).

To rule out potential effects caused by the $SH3PX1^{d1/d1}$ genetic background, another null allele, $SH3PX1^{HK62b}$, was utilized (Knaevelsrud et al., 2013) (Figure S1A). Trans-heterozygous $SH3PX1^{d1/HK62b}$ mutants showed an ISC mitotic phenotype similar to $SH3PX1^{d1/d1}$ mutants (Figures 1C and S1C), confirming that SH3PX1 is specifically restrains ISC divisions. To further assess the intestinal role of SH3PX1, SH3PX1 protein was visualized using an anti-SH3PX1 antibody (Worby et al., 2001). SH3PX1 was expressed in all cell types in the midgut, membrane localized, and showed relatively high amounts in *escargot*-positive (esg^{+}) progenitor cells (ISCs + EBs; Figure 1D). Interestingly, enteric infection with *Pseudomonas entomophila* (*P.e.*), which damages the gut epithelium and results in faster regenerative growth (Jiang et al., 2009), disrupted the membrane-associated pattern of SH3PX1 (Figure 1D, lower panels), suggesting that proper subcellular localization of SH3PX1 might be required for intestinal homeostasis and normal regeneration.

We next tested whether SH3PX1 functions in a cell autonomous or non-autonomous manner to control ISC proliferation, using different cell type-specific Gal4 “drivers” to express *RNAi* targeting *SH3PX1*. Knockdown of *SH3PX1* using two independent *RNAi* strains driven by the ISC-specific driver esg^{ts} *Su(H)GBE-Gal80* generated large increases in ISC mitoses similar to those seen in the null mutants (Figures 1E–1F). Knockdown of *SH3PX1* using the EB-specific driver $Su(H)GBE^{ts}$ slightly increased the $pH3^{+}$ cell numbers (Figure S1D), consistent with a previous observation that a small population of EBs maintains

proliferative capability (Jin et al., 2015). However, depleting *SH3PX1* in ECs (via the $Myo1A^{ts}$ driver), or in EEs (via the $ProsV1^{ts}$ driver), had no effect on ISC mitoses (Figures S1E–S1F), indicating that SH3PX1 functions cell-autonomously to regulate ISC proliferation. As expected, expression of *SH3PX1* in progenitor cells successfully rescued the ISC over-proliferation defect and lifespan deficit in homozygous $SH3PX1^{d1/d1}$ mutants (Figure 1G). Moreover, *esgGal4*-driven *SH3PX1* expression also rescued the lifespan defect in these mutant flies (Figure 1H), indicating that the mortality of $SH3PX1^{d1/d1}$ mutants was due primarily to midgut progenitor cell hyperplasia.

Previous studies showed that blocking differentiation (*e.g.*, by *Notch* mutation) causes ISC hyperproliferation. To rule out the possibility that $SH3PX1^{-/-}$ promotes ISC mitosis by blocking differentiation, $SH3PX1^{d1}$ mutant MARCM clones were generated and stained for the differentiation markers Pdm1 (an EC marker) and Prospero (an EE marker). Both Pdm1 and Prospero (Figures S3D–S3D“) were present at normal frequencies inside $SH3PX1^{d1/d1}$ mutant clones, indicating that SH3PX1 loss does not block differentiation. Thus SH3PX1 specifically restrains ISC proliferation.

SH3PX1-dependent autophagy restricts ISC proliferation

SH3PX1 and its human ortholog *SNX18*, have been reported to be positive regulators of autophagosome formation (Knaevelsrud et al., 2013). To determine whether SH3PX1 controls ISC proliferation by affecting autophagy, an *esgGal4>UASp-GFP-mCherry-Atg8a* fly line was generated to visualize autophagosome formation in ISCs and EBs. After 6hr starvation, autophagosomes were clearly observed in the ISCs of heterozygous $SH3PX1^{d1/+}$ flies but not in homozygous $SH3PX1^{d1/d1}$ flies (Figure 2A). This indicated that SH3PX1 is required in ISCs for autophagosome formation, and suggested that other mediators of autophagy might also restrain ISC proliferation. Indeed, *RNAi*'s directed against the autophagy-related genes *Atg1, 5, 6, 7, 8a, 9, 12* and *16* significantly increased ISC proliferation when expressed in progenitor cells (Figures 2B–2C). Depletion of *Syntaxin 17* (*Syx17*), a regulator of autophagosome-lysosome fusion (Takats et al., 2013), also promoted ISC proliferation (Figure 2B). As these *Atg* genes control different steps in the autophagy pathway (Mulakkal et al., 2014), we conclude that SH3PX1 restricts ISC proliferation by promoting autophagy.

Previous studies indicated that multiple stages of endocytic flux are also essential for efficient autophagy (Tooze et al., 2014), raising the possibility that endocytic vesicle trafficking also controls ISC proliferation. Two key regulators of endocytosis, Rab5 and Rab7, were tested. Overexpression of $Rab5^{SN}$, a dominant negative form of *Rab5* (Strutt et al., 2011), via the esg^{ts} driver led to a striking increase of ISC mitoses (Figure 2D). Similarly, *RNAi* targeting *Rab7* in progenitor cells also promoted proliferation (Figure 2D). Thus inhibition of endocytosis also leads to ISC hyperproliferation.

The proliferative phenotypes that arise from these disruptions of endocytic traffic could be due to excessive accumulation of mitogenic cargoes (*e.g.*, activated transmembrane receptors) that are normally degraded via autophagy. If fluxes in the endocytosis/autophagy network were reversed due to blockages, mitogenic cargoes might accumulate in the active form in various endocytic compartments or be recycled to the cell surface. There are two

well characterized endocytic recycling pathways: a Rab4-mediated fast route directly from early endosomes, and a slow Rab11-mediated route from perinuclear recycling endosomes (Guichard et al., 2014). ISC-specific knockdown of *Rab11* strikingly repressed the hyperproliferation caused by *SH3PX1* depletion (Figure 2E). However, overexpression of $Rab4^{SN}$, a dominant negative form of *Rab4* (Strutt et al., 2011), did not (Figure 2E). Consistently, knockdown of *Rab11* also repressed ISC mitoses caused by $Rab5^{SN}$, $Rab7^{RNAi}$, $Atg1^{RNAi}$ and $Syx17^{RNAi}$ (Figures 2D–2F). These data indicate that Rab11-mediated recycling endosomes play an important role in triggering ISC mitosis following endocytosis/autophagy disruption. This may be because Rab11 endosomes are required to return active, mitogenic cargoes to the plasma membrane, or because such cargoes only remain active in Rab11 endosomes.

Next, we asked whether autophagy and endocytosis work together or in parallel to control ISC proliferation. To this end, an epistasis test was performed between *SH3PX1* and the *Drosophila* dynamin homolog *shibire (shi)*, which is required at the initial step of endocytosis. Overexpression of shi^{TS}, a temperature-sensitive dominant negative mutant form of *shi* (Kitamoto, 2001) using the esg^{ts} driver moderately increased ISC mitoses (Figure 2G). This is consistent with the idea that blocking endocytosis stabilizes growth factor receptors or other mitogenic factors at the plasma membrane, thereby promoting ISC proliferation. If shi-dependent endo-lysosomal degradation works in parallel with SH3PX1-dependent autophagy, overexpression of shi^{TS} in conjunction with $SH3PX1^{RNAi}$ would be expected to have additive effects on ISC mitoses. Contrary to this expectation, expression of shi^{TS} suppressed midgut ISC mitoses caused by $SH3PX1^{RNAi}$ (Figure 2G). This suggests that the mitogenic cargoes that accumulate after SH3PX1 dysfunction likely originate, at least in part, from early endocytosis at the plasma membrane. From this, we surmise that autophagy and endocytosis work together to restrain ISC proliferation.

Autophagy restrains ISC division by dampening EGFR/ERK activity

To elucidate which downstream effectors of SH3PX1-dependent autophagy are responsible for inducing ISC proliferation, we did epistasis tests between SH3PX1 and signaling pathways known to promote ISC division. These included the insulin/PI3K, JAK/STAT, JNK, wingless, and EGFR pathways. Silencing each of these pathways could suppress ISC mitosis caused by *SH3PX1* depletion (Figure 3A). However, in most cases these inhibitory effects diminished over time (Figures 3A and S4A). Silencing of the EGFR pathway by *MEK* depletion, however, gave a singularly strong and persistent inhibitory effect (Figures 3A and S4A), suggesting that EGFR signaling may be dominant to the other pathways. To further test the primacy of EGFR signaling, the epistatic relationships of SH3PX1 with other components of the pathway (EGFR, Ras, pointed (pnt) and Ets21C) were tested (Jin et al., 2015). Suppressing any of these genes' functions strongly and permanently repressed $SH3PX1^{RNAi}$-driven ISC mitoses and intestinal dysplasia (Figures 3B–3C). Furthermore, ISC mitoses induced by deficiencies in autophagy ($Atg1^{RNAi}$, $Atg8a^{RNAi}$ and $Syx17^{RNAi}$) could also be blocked by the depletion of EGFR pathway components (Figures 3D and S5A). These data suggest that EGFR signaling is a major downstream target of SH3PX1-dependent autophagy.

Because these results suggest that dysfunction in any step of the endocytosis/autophagy network may trigger hyperactivation of EGFR signaling, the activation of the principal EGFR effector, mitogen-activated protein kinase (MAPK), was examined by staining for active, di-phosphorylated ERK (dpERK). Indeed, dpERK signals were strikingly induced in *SH3PX1*$^{d1/d1}$ mutant midguts (Figure 3E). *RNAi*-mediated *SH3PX1* depletion also increased the levels of dpERK (Figure S5B), predominantly in the targeted *esg*$^{+}$ progenitor cells. Consistently, *RNAi* expression targeting either autophagic flux (*esg*^{ts}*>Atg1*^{RNAi}, *Atg8a*^{RNAi}, *Syx17*^{RNAi}) or endocytosis (*esg*^{ts}*>Rab5*^{SN}, *Rab7*^{RNAi}) in progenitor cells induced high levels of dpERK, similar to the effects of *SH3PX1* loss (Figures 3F and S5D).

Further tests showed that two other receptor tyrosine kinases expressed in the midgut, fibroblast growth factor receptor (FGFR) and PDGF/VEGF receptor (PVR), were not important for MAPK activation following *SH3PX1* loss (Figure S5C). Similarly, *SH3PX1*^{RNAi} was fully capable of activating dpERK in ISCs depleted of Insulin Receptor (InR), the Upd cytokine receptor (Dome), JNK, or the Wnt effector Pangolin (TCF) (Figure S4B). Altogether these data indicate that EGFR/ERK signaling is directly activated as a result of autophagy dysfunction.

EC-localized stress signaling is dispensable for proliferation of *SH3PX1* mutant ISCs

Two possible mechanisms of MAPK activation following *SH3PX1* loss were examined: In the first scenario, EGFR/Ras/MAPK signaling is a direct cell autonomous target of SH3PX1-dependent autophagy. In the second, dysfunction of SH3PX1-dependent autophagy causes ISC proliferation via a different mechanism, but proliferating ISCs stress the gut epithelium, which leads to the production of Unpaired cytokines, EGFR ligands, and Rhomboids (Jiang et al., 2011), thus triggering EGFR/Ras/MAPK signaling in indirectly. This second, non-cell autonomous mechanism is well documented in the fly gut (Jiang et al., 2011; Patel et al., 2015; Xiang et al., 2017). Previous studies have demonstrated that the JNK and Hippo pathways are major inducers of the cytokines Unpaired 2 and 3 (Upd2, 3) following stress (Jiang and Edgar, 2011), and that Upd/Jak/Stat signaling can secondarily promote EGFR signaling (Jiang et al., 2011). We first examined the activity of the Hippo/Yki pathway. In the R4 region of wild-type midguts, the Yki target, *ex-lacZ*, showed weak expression in ECs and was absent in ISCs (Figure 4A, upper panel). In contrast, loss of *SH3PX1* in progenitor cells markedly increased *ex-lacZ* levels in ECs (Figure 4A, lower panel). To determine whether Yki activation was responsible for ISC proliferation in the context of *SH3PX1* loss, we depleted *yki* in ECs using an *RNAi*. In this case, ISCs mitoses in the *SH3PX1*$^{d1/d1}$ mutants were significantly reduced (Figure 4B). Given that Yki can upregulate Upd2 and Upd3 in ECs (Shaw et al., 2010), we tested the induction of Upd3 using the *upd3-lacZ* reporter (Jiang et al., 2009). As expected, *upd3-lacZ* was exclusively upregulated in ECs surrounding *SH3PX1*-depleted progenitors (Figure 4C, lower panel). To determine whether Upd induction contributes to ISC proliferation in *SH3PX1* mutant, we removed both *upd2* and *upd3* using a viable deletion mutant, and found that ISC mitoses in the *SH3PX1*$^{d1/d1}$ mutants were significantly reduced (Figure 4D). This repression was attenuated over time, however (Figure 4D) and moreover, in *upd2*$^{\Delta}$,*3*$^{\Delta}$; *SH3PX1*$^{d1/d1}$ mutant midguts, we still observed massively high dpERK signals in the hyperproliferative progenitor cells (Figure 4E). These results indicate that while the Upd2 and 3 cytokines are

induced and contribute to *SH3PX1*$^{-}$-driven hyperplasia, cytokine signaling is not essential for the hyperplasia or for EGFR activation.

These observations raised the possibility that other EC-derived mitogens might promote ISC mitoses. Several Rhomboid (Rho) proteases are induced in stressed ECs, and these promote the cleavage and secretion of EGFR ligands Spitz (Spi) and Keren (Krn) (Jiang et al., 2011; Liang et al., 2017). Consistently, we found that *rho-lacZ*, a *rhomboid* transcriptional reporter, was highly induced in ECs surrounding *SH3PX1*-depleted progenitors (Figure 4F). To test whether *rho* and its substrates were required for ISC activation, we depleted either *rho* or *Krn* in ECs using *RNAi*, in the *SH3PX1*$^{d1/d1}$ mutant background. This failed to repress the ISC divisions caused by *SH3PX1* loss (Figures 4G–4H), suggesting that the paracrine induction of *rho* and secretion of Krn from ECs are not required for ISC hyperproliferation. Since the induction of dpERK activity in ECs was observed in most cases of endocytosis/autophagy dysfunction (Figures 3F, 5E, S4B, S5B and S5D), we tested whether *RNAi*-mediated suppression of *MEK* in ECs might affect ISC activation in *SH3PX1* mutants. While *MEK*^{RNAi} effectively blocked ERK activity in ECs (Figure 5E), it did not suppress ISC-autonomous ERK activation or mitoses (Figure 5D, E). Overall these data indicate that stress signaling within and from ECs is dispensable for ISC mitoses triggered by *SH3PX1* mutations.

Cell autonomous EGFR/Ras/MAPK activation triggers *SH3PX1*$^{-}$-ISC division

Given these findings, we inferred that ISC-autonomous EGFR/Ras/MAPK activation was the primary trigger of hyperplasia in the *SH3PX1* mutants, and that the induction of Yki-, Upd3-, and Rho-reporters in ECs was likely a secondary consequence of ISC hyperplasia. To test this hypothesis, we blocked ISC mitoses using an *RNAi* against *String (stg)*, a *Cdc25* homolog required for all somatic cell mitoses in *Drosophila* (Edgar and O'Farrell, 1989). Co-expressed *stg*^{RNAi} completely blocked ISC mitoses caused by *SH3PX1*^{RNAi} (Figure 5A), and also suppressed the induction of *upd3-lacZ* and *rho-lacZ* (Figure 5B). Similarly, *MEK*^{RNAi} expressed in *SH3PX1*-mutant ISCs blocked mitoses and the induction of *upd3-lacZ* and *rho-lacZ* in ECs (Figure 5C). These results confirm that it is the hyperproliferation of *SH3PX1*-mutant ISCs that induces stress-dependent mitogenic signaling from ECs. Importantly however, even when epithelial stress was pre-empted by blocking ISC mitoses with *stg*^{RNAi}, activation of dpERK was still observed in the *SH3PX1*-mutant ISCs (Figure 5F). Thus, all of our data are consistent with the idea that ISC-autonomous activation of EGFR/Ras/MAPK signaling is the primary trigger for ISC mitoses in cases of endocytosis-autophagy dysfunction.

SH3PX1 regulates EGFR signaling via multiple mechanisms

We next considered how blockages in the endocytosis/autophagy network might activate EGFR/Ras/MAPK signaling in ISCs. To assess EGFR expression in the fly midgut we used *esg*^{ts}*F/O*, a lineage induction system that labels ISCs and all their newborn progeny after a temperature shift (Jiang et al., 2009). Consistent with our previous observations (Xiang et al., 2017), we noted that EGFR is highly expressed in ISCs and EBs and strongly reduced in ECs (Figure 6A, left), suggesting that it is down-regulated as progenitor progeny differentiate. Surprisingly, overexpression of *EGFR* with *esg*^{ts}*F/O* gave essentially the same

expression pattern (Figure 6A, middle), even though this induction system drives the transcription of *EGFR* in ECs as well. This suggests that the stability of EGFR protein must be reduced as progenitor cell progeny differentiate. Remarkably, in *esg^{ts}F/O>SH3PX1^{RNAi},EGFR^{wt}* midguts, EGFR protein became visible in newborn ECs (Figure 6A, right). This implies that EGFR is likely stabilized by *SH3PX1* depletion, and thus that SH3PX1-dependent autophagy promotes EGFR degradation. Stabilization of activated EGF receptors, either at the plasma membrane or in endosomes, may be one mechanism via which ERK is activated by blocking flux through the endocytosis-autophagy network.

Notwithstanding these findings, overexpressing *EGFR^{wt}* in progenitors produced a consistently weaker mitotic phenotype than *SH3PX1^{RNAi}* (Figure 6B), suggesting that *SH3PX1* loss might potentiate ERK signaling via additional mechanisms. Previous studies show that two autocrine EGFR ligands, Spi and Krn, are expressed by ISCs (Buchon et al., 2010; Jiang et al., 2011; Patel et al., 2015). Cleavage and secretion of Spi and Krn require the intramembrane protease, Rhomboid (Rho). We thus examined whether Rho, Spi, and Krn were required for *SH3PX1^{RNAi}*-dependent EGFR/Ras/MAPK activation. Whereas ISC-targeted *RNAi* against *spi* did not inhibit *SH3PX1^{RNAi}*-dependent mitoses, suppressing either *rho* or *Krn* did (Figures 6C–6E). These results suggest that ISC-produced Rho and Krn potentiate the activity of EGFR, which is stabilized by dysfunctions in autophagy. Considering the importance of Krn and Rho, we note that the activity of these factors might also be affected by impairing autophagic flux. Notably, the over-expression of *rho* in ISCs was sufficient to trigger mitoses (Figure 6F), suggesting the cleavage of Krn may be a limiting step for EGFR activation in ISCs, and the proliferative effect of overexpressed *rho* was suppressed by knockdown of *Rab11* (Figure 6F), which has been shown to be required for the recycling of EGFR (Cullis et al., 2002). Taken together, these data suggest that in SH3PX1 mutant ISCs, Rho-activated Krn but not Spi may activate EGFR in Rab11 endosomes, thereby initiating ISC mitoses.

Since autophagy functions as a non-canonical Endoplasmic Reticulum-Associated Degradation (ERAD) pathway (Senft and Ronai, 2015), the perturbation of SH3PX1-dependent autophagy might cause retention of proteins in the ER, triggering ER stress. We assessed this possibility by monitoring ER stress in *SH3PX1*-depleted midguts using the *UAS-xbp1-EGFP* reporter, in which EGFP is expressed in frame only upon ER stress (Ryoo et al., 2007). This test indicated that *SH3PX1^{RNAi}* apparently triggered ER stress (Figure S6). Further, as ER stress can trigger Calcium release from ER stores (Deniaud et al., 2008), we used *UAS-GcaMP6s*, a Ca^{2+} reporter (Xu et al., 2017), to record intracellular Ca^{2+} flux in midgut progenitor cells. Relative to controls, *SH3PX1^{RNAi}* expressing progenitors displayed reduced Ca^{2+} oscillation frequencies but longer peaks of high Ca^{2+} activity (Figures 6G–6H), suggestive of increased overall Ca^{2+} signaling. A recent study showed that high cytosolic Ca^{2+} is necessary and sufficient to activate ERK and mitosis in ISCs, and that EGFR was required for this effect (Xu et al., 2017). Consistent with this mechanism, we found that *esg^{ts}*-driven *RNAi* targeting either *transient receptor potential A1 (TRPA1)*, a plasma membrane Ca^{2+}-permeable cation influx channel (Xu et al., 2017), or *ryanodine receptor* (*RyR*), an ER-localized cation channel that releases Ca^{2+} into the cytosol (Xu et al., 2017), strongly suppressed ISC mitoses caused by *SH3PX1* depletion (Figure 6I). These data suggest that SH3PX1 may deregulate EGFR/Ras/MAPK signaling by perturbing

intracellular calcium fluxes. Altogether, our data indicate that dysfunctions in endocytosis/autophagy network activate EGFR/Ras/MAPK signaling via multiple inputs.

Autophagy mutations are associated with MSI-H and CIMP-H colorectal cancers

To test whether the restriction of EGFR/Ras/MAPK activation via the SH3PX1-dependent endocytosis/autophagy network is a conserved process from insects to humans, we generated transgenic flies carrying human *SNX9*, *18* and *33* genes, and tested their ability to rescue *SH3PX1* mutant phenotypes in the *Drosophila* midguts. The tests showed that human *SNX9*, *18*, or *33* could effectively rescue *Drosophila SH3PX1*'s loss-of-function phenotype in ISCs (Figure 7A), confirming that *Drosophila* SH3PX1 is functionally conserved with human *SNX9*, *18* and *33* genes.

Next, we examined the ability of autophagy to restrain EGFR/ERK signaling in cultured human Retinal Pigment Epithelial (RPE-1) cells (Spalluto et al., 2013) and CaCo-2 (*KRAS/BRAF* wild-type) colon cancer cells (Ahmed et al., 2013). Consistent with our results from *Drosophila*, depressing autophagy in either cell line using the autophagy inhibitors, 3-MA (Figures 7B–7C) or Thapsigargin (TG) (Figures S7A–S7B), rapidly increased dpERK levels. Further, 3-MA treatment caused a rapid accumulation of EGFR in RPE-1 cells (Figures 7D–7E). This indicates that, as in *Drosophila*, autophagy can restrain EGFR/ERK signaling in human cells.

Given that genetic and epigenetic aberrancies that dysregulate epithelial homeostasis contribute to malignancy (Pesic and Greten, 2016), we examined mutation data of 15 human endocytosis/autophagy network genes orthologous to the genes we characterized in *Drosophila* (Table S1). Analysis of The Cancer Genome Atlas (TCGA) datasets by cancer type indicated that the colorectal adenocarcinoma and other cancers harbor a high frequency of mutations and deep deletions in these genes (Figure 7F, Table S2). From a colorectal adenocarcinoma (DFCI) gene set we found that, *ULK1*, the human ortholog of *Atg1*, and *SNX18* and *SNX33* were the most frequently mutated endocytosis/autophagy genes in CRC (Figure 7G, Table S3). This is consistent with the proposition that CRCs harbor frameshift mutations in autophagy genes (Choi et al., 2017), and suggests that the endocytosis/autophagy network may play a critical role in human colorectal carcinogenesis. We next assessed the degree to which somatic mutations in the endocytosis/autophagy genes are related to other genomic and epigenomic changes in human CRC. Classification according to microsatellite instability demonstrated that mutations in the endocytosis/autophagy network were significantly enriched among MSI-H CRC samples (Figure 7H, Table S4). These samples also showed a strong association between endocytosis/autophagy pathway mutations and CIMP-H status, an epigenomic CRC phenotype that underlies sporadic microsatellite instability (Figure 7I, Table S5) (Issa, 2004; Weisenberger et al., 2006). Finally, we found that mutations in the three human orthologs of *Drosophila SH3PX1* (*SNX9/18/33*) have a negative association with *KRAS* activating mutations in CRCs (Figure 7J, Table S6). This suggests an alternative route to RAS-ERK activation that may underlie novel CRC diagnostic and therapeutic strategies. We suggest that dysfunction in the endocytosis/autophagy network, acting at least partially through SNX-dependent autophagy and activated *KRAS* signaling, may promote human colorectal carcinogenesis.

DISCUSSION

Exocytic and endocytic pathways are known to play crucial roles in signal transduction during normal and pathophysiological processes (Gissen and Maher, 2007), but how these pathways impact the behavior of stem cells or epithelial homeostasis has not been extensively explored. In *Drosophila*, just one relevant study shows that the vesicle-mediated COPI-Arf79F complex is required for intestinal stem cell (ISC) survival (Singh et al., 2016). Here, we identify a novel mechanism by which SH3PX1-dependent vesicle trafficking regulates EGFR/Ras/MAPK activity and ISC behavior. A large set of endocytosis and autophagy genes act to contain EGFR signaling in multiple ways. These include de-stabilizing the EGFR, limiting ligand (Krn) function, and dampening cytosolic Ca^{2+} signaling, all of which act to restrain ISC proliferation. These mechanisms are of such importance in ISCs that blockages in endocytic flux drastically upregulate basal EGFR/Ras/MAPK activity, promoting ISC proliferation, gut epithelia hyperplasia, and eventual death of the organism. While published data show that the endocytosis factors Dynamin (Vieira et al., 1996), Rab GTPases (Ceresa, 2006), and SNX1, 9 and 16 (Choi et al., 2004; Kurten et al., 1996; Lin et al., 2002) mediate EGFR degradation, only one paper showed enhanced signaling activity (ERK phosphorylation) following endocytic flux inhibition (Vieira et al., 1996), and none of the relevant papers report effects on cell proliferation or stem cell activation, centrally important functional consequences. Further, to our knowledge, no previous reports attribute endocytosis-mediated degradation of EGFR to autophagy.

Autophagy has been viewed as a “double-edged sword” in cancer because it can be either tumor suppressive or oncogenic, depending upon cancer type and stage (White and DiPaola, 2009). In early carcinogenesis, as in our study, autophagy can be tumor suppressive by degrading oncogenic proteins and limiting genotoxic stresses that promote cancer progression (Kondo et al., 2005). In the later stages of carcinogenesis, however, autophagy can act oncogenically by providing recycled nutrients to sustain cancer metabolism (Kondo et al., 2005). Recent studies in the mouse intestine report that autophagy genes (*ATG5*, *ATG7* and *ATG16L1*) are necessary for ISC maintenance and CRC progression (Asano et al., 2017; Levy et al., 2015; Matsuzawa-Ishimoto et al., 2017), but these studies used the pan-iEC recombinase, *Villin-Cre*, making it impossible to distinguish ISC-autonomous requirements from functions in other epithelial cell types such as enterocytes. In contrast, our study in the fly gut shows that ISC-autonomous defects in autophagy can release stem cell proliferation without regulating differentiation, potentially increasing cancer risk. Further, as in other studies of the fly intestine, we found that hyperproliferative stem cells can stress the surrounding epithelium and induce widespread mitogenic signaling, which in turn catalyzes a feed-forward loop that drives massive hyperplasia of the mutant stem cells. The model we propose here places the SH3PX1-dependent endocytosis/autophagy network at the nexus of this feed-forward loop, a situation that may also play out in human cancers.

Previous literature addressing autophagy and *Drosophila*’s ISCs is sparse, and offers divergent conclusions. One study (Nagy et al., 2016) reported that UVRAG, a known regulator of autophagy, restricts ISC proliferation independent of autophagy. They also published a follow-up study showing that knockdown of other *Atg* genes adversely affected ISC maintenance (Nagy et al., 2018). That study, however, did not test the majority of *Atg*

genes investigated here, and moreover our data are consistent with another report (Zeng et al., 2015) showing that loss of *Atg2* or *Atg6* promotes ISC hyperproliferation. Consistently, Thapsigargin, a drug that arrests autophagy by blocking autophagosome-lysosome fusions (Ganley et al., 2011), also stimulates ISC mitosis (Deng et al., 2015). Taken together, Nagy *et al's* findings and our contrasting results suggest that the specific *Atg* gene that is inhibited may differentially affect proliferation vs. stem cell maintenance. Indeed autophagy is known to employ different genetic components in different cell types (Chang et al., 2013; Wen et al., 2017), and some *Atg* genes have autophagy-independent functions (Tang et al., 2013).

Elucidating the specific cargos of the SH3PX1-dependent network that mediate its effects on ISCs proved to be challenging. Using genetic tests we were able to rule out several mitogenic signaling pathways as secondary and involved non-cell autonomously, and to identify EGFR/ERK signaling as the primary, cell autonomous trigger for *SH3PX1*$^{-}$-dependent ISC proliferation. The importance of this pathway is expected, as previous studies show that EGFR/ERK signaling is both universally required and sufficient to activate *Drosophila* ISCs for growth (Jiang et al., 2011; Jin et al., 2015; Xiang et al., 2017; Xu et al., 2017). Of note, our genetic tests showed that *RNAi* against *Rab11*, a small GTPase critical for recycling endosome function, dominantly suppressed ISC mitoses induced by any other endocytosis/autophagy network defect. Further, we found that *SH3PX1*$^{-}$-dependent ISC proliferation requires the EGFR ligand, Krn, and the Rho intramembrane protease that cleaves and activates it. This suggests that *SH3PX1* loss drives the accumulation of activated, Krn-bound EGFR complexes in Rab11 recycling endosomes and/or at the plasma membrane, thereby constitutively activating downstream signaling. This conclusion is supported by reports that clathrin-mediated endocytosis and the endosomal localization of EGFR sustain pathway activation (Sigismund et al., 2008; Sorkin and Von Zastrow, 2002). Unfortunately, due to a lack of reagents, we were unable to test for increased co-localization of Krn and EGFR in Rab11 endosomes. Future studies detailing how defects in endocytic flux affect the distribution and accumulation of EGFR pathway components in the various endosomal compartments should extend the general model we propose here.

SNX, RAB and ATG proteins are highly conserved, yet the genomic status of these genes in human disease is largely unexplored. Using TCGA data, we uncovered a strong association between colorectal tumors with somatic mutations in *ATG* and *SNX* genes, and MSI-H and CIMP-H status. Consistent with this, the DNA damage-activated kinase Chk2 (Checkpoint kinase 2) is upregulated by *Atg6* knockdown (Nagy et al., 2018), suggesting that dysfunctions of autophagy might promote genomic instability. In addition, one previous study found that frameshift mutations in nucleotide repeats in human *ATG5*, *ATB9B*, and *ATG12* were highly enriched in MSI-H CRCs (Kang et al., 2009), and another came to a similar conclusion regarding *ULK1* (*ATG1A*) and *ULK2* (*ATG1B*) (Choi et al., 2017). These reports suggest that aberrancies in *ATG* and *SNX* genes are linked to the distinct MSI-H/CIMP-H molecular phenotype found in a subset of CRCs. The association with MSI-H may simply reflect the fact that all of the *ATG* and *SNX* genes that show the association (Figure 7H) contain long (>7 nucleotide) mono-nucleotide repeats in their open reading frames and become very mutable when defects in the DNA mismatch repair arise, as is the case in MSI-H CRC. The association could also reflect more complex unknown functional interactions between endocytosis/autophagy and mismatch repair genes. Either way, the

differential response of MSI-H CRCs to chemotherapeutic regimes illuminates an issue that could form the basis for novel cancer diagnostics or therapies involving autophagy (Vilar and Gruber, 2010).

The molecular phenotyping of CRCs for CIMP status is also an integral prognostic classifier in patients (Toyota et al., 1999). Transcriptional inactivation by cytosine methylation at promoter CpG islands in tumor suppressor genes is believed to be an important mechanism in human colorectal carcinogenesis (Ogino and Goel, 2008), and CIMP-H tumors represent a distinct etiologic and clinical CRC phenotype (Issa, 2004). Although no studies to date have examined CpG island methylation at promoter regions of the endocytosis and autophagy genes in CRC, the downregulation of *ULK1* and *ULK2* via promoter hypermethylation is critical to inhibit autophagy and promote tumor development in CIMP-H glioblastoma (Shukla et al., 2014). Our findings suggest that this association may apply in CRC and other cancers.

EGFR is overexpressed in 49–82% of CRCs (Antonacopoulou et al., 2008), and in cancers with EGFR activation, EGFR-specific antibodies such as cetuximab can suppress cell growth by blocking ligand-induced receptor signaling (Jonker et al., 2007). However, this efficacy is limited (Pozzi et al., 2016) and the activation mechanisms of EGFR signaling are only understood in a subset of cancers, most notably those with activating *KRAS* or *BRAF* mutations. Our findings suggest that EGFR/ERK signaling may also be activated by loss-of-function in *SNX*, *RAB* and *ATG* genes. We uncovered a negative association between mutations in the human *SH3PX1* homologues *SNX9/18/33* and activating mutations in *KRAS* in CRC patients, suggesting that this alternative route to ERK activation may be at play in some tumors. This and other studies addressing how EGFR signaling is activated in cancer stem cells that lack *KRAS* and *BRAF* mutations may help develop new strategies for suppressing ERK signaling in CRC and other EGFR-dependent cancers.

STAR METHODS

CONTACT FOR REAGENT AND RESOURCE SHARING

Requests for resources and reagents should be directed to and will be fulfilled by the Lead Contact, Bruce A. Edgar (bruce.edgar@hci.utah.edu).

EXPERIMENTAL MODEL AND SUBJECT DETAILS

All fly strains were kept on standard fly medium at 25°C. For temperature shift experiments, flies were raised at 18°C prior to shifting to the temperature conditions described in the corresponding figure legends and method details. Midguts were dissected from adult females, except in Figure 4D.

Human SNX transgenic flies—The cDNA of *hSNX9*, *hSNX18* and *hSNX33* were cloned into the *pUAST-attB-V5* vector, respectively. *UAS-hSNX9*, *UAS-hSNX18* and *UAS-hSNX33* were generated using PhiC31 integrase-mediated site-specific transgenesis system.

Fly Diet—For 1L: 18g active dry yeast, 61g corn meal, 15ml syrup, 81.5g malt and 11.2g agar. Ingredients were mixed well with water and brought to boil in kettle. After cooling,

7.5ml of 99.5% propionic acid (Sigma-Aldrich) and 10ml Tegosept (methyl 4-hydroxybenzoate in 95% ethanol at 100g/L, Sigma-Aldrich) were added to the mixture and the solution was dispensed into vials/bottles.

Cell culture—Human RPE-1 (female) and CaCo-2 (male) cell lines were cultured in DMEM/F12 (Gibco) supplemented with 10% FBS (Gibco) and 100U/ml penicillin/streptomycin (Gibco) in a sterile humidified 37°C incubator with 5% CO_2 atmosphere.

Bacteria culture—*Pseudomonas entomophila* (*P.e.*, gift from Nicolas Buchon), a gram-negative bacterium that naturally infects *Drosophila* (Vodovar et al., 2005), was grown in LB medium (400μL *P.e.* glycerol stock in 200mL LB) containing Rifampicin (100μg/mL) at 29°C with shaking at 130rpm for 48hr. The culture was centrifuged at 2500g for 25min at 4°C and the resultant pellet was resuspended in 8mL 5% sucrose for fly oral infection.

METHOD DETAILS

Bacterial infection—For oral bacterial infection, 2–3 day-old adult flies were shifted from 18°C to 29°C and raised for 2d on normal fly food before infection. Flies were then transferred to empty vials containing Whatman paper discs soaked with an infection solution (*P.e.* pellet resuspended with 5% sucrose) or a control solution (5% sucrose). Yeast paste made with the above control or infection solution was also provided on the wall of the vials. Flies were orally infected for 16hr at 29°C and then subjected for dissection.

Immunostaining—After dissection, samples were fixed in PBS with 4% paraformaldehyde for 30min, washed in PBS with 0.1% Triton X-100, and blocked in PBS with 0.1% Triton X-100 and 10% NGS for at least 30 min at room temperature. For the dpERK and EGFR staining, to ensure consistent staining, the midgut samples were first fixed in 8% paraformaldehyde, followed by a critical methanol (−20°C, 10min) fixation step. All samples were then stained with primary antibodies at 4°C overnight with the following dilutions: chicken α-GFP (Thermo Fisher Scientific, 1:1000), rabbit α-DsRed (Clontech Laboratories, 1:500), rabbit α-PH3 (Millipore, 1:1000), mouse α-PH3 (Cell Signaling Technology, 1:300), rabbit α-phospho-p44/42 MAPK (Erk1/2) (Cell Signaling Technology, 1:200), mouse α-β-gal (Promega, 1:500), mouse α-EGFR (Sigma-Aldrich, 1:100), rabbit α-SH3PX1 (gift from Jack Dixon, 1:300), mouse α-Prospero (DHSB, 1:50), rabbit α-Pdm1 (gift from Xiaohang Yang, 1:200).

DAPI (Thermo Fisher Scientific, 1:1000) was used to label nuclei. Staining was detected by Alexa Fluor 488, 568, or 633 conjugated species appropriate secondary antibodies (Thermo Fisher Scientific, 1:1000).

Western blot—Cell lysates were prepared in 2× SDS Loading Buffer (80 mM Tris pH6.8, 2% SDS, 12% glycerol, 10% β-mercaptoethanol, bromophenol blue). For the western blot shown in Figure S1B, three adult flies per sample were homogenized by grinding in 200 ul 2× SDS Loading Buffer. Lysates were boiled and clarified by centrifugation before analysis by western blotting. Primary antibodies used for western blotting were: rabbit anti-SH3PX1 (gift from Jack Dixon, 1:1500), mouse anti-α-tubulin (DSHB 12G10, 1:10,000), mouse anti-p44/42 MAPK (Erk1/2) (Cell Signaling Technology, 1:1500), rabbit anti-phosphop44/42

MAPK (Erk1/2) (Cell Signaling Technology, 1:3000), mouse anti-vinculin (Sigma-Aldrich, 1:5000), rabbit anti-EGFR (Cell Signaling Technology, 1:2000).

Live-imaging and cytosolic Ca^{2+} measurements—Live-imaging experiments were performed using 3–5d old flies with the following genotypes: *esg^{ts},UAS-GCaMP6s>w1118* and *esg^{ts},UAS-GCaMP6s>SH3PX1^{RNAi-1}*. Flies were raised at 18°C. Adult females were shifted to 29°C after eclosion for 4d before dissection in adult hemolymph-like (AHL) saline (108 mM NaCl, 25 mM KCl, 2 mM $CaCl_2$, 8.2 mM $MgCl_2$, 4 mM $NaHCO_3$, 1 mM NaH_2PO_4, 5 mM trehalose, 10 mM sucrose, and 5 mM HEPES pH 7.5). Three explanted intact midguts were placed in a clear bottom plastic well from a 4-well chambered slide (IBIDI, Cat#80426), carefully oriented with forceps, and gently covered with a piece of mixed cellulose esters membrane (Millipore, AABP02500) to keep them in place. The well was then filled with 0.5 ml of AHL containing 10 μg/mL Isradipine so as to minimize visceral muscle movement. For each condition, 2 replicates were produced, each consisting in the measurement of 3 midguts. Each midgut was imaged separately using a Nikon (Eclipse T*i*) widefield microscope or a Leica SP8 confocal microscope with comparable results. A Z-stack encompassing a 60–100μm section of the posterior midgut with a Z-step of 10 μm was captured every 10” for a total live-imaging duration of 10’. Images were processed in ImageJ using a custom macro. Briefly, movies were stabilized using the StackReg plugin so as to compensate for residual midgut movements, and a maximum intensity projection was produced which was used for the subsequent analysis. Cells expressing GCaMP6s that were clearly visible for the whole imaging duration were then selected, and their mean fluorescence intensity was manually calculated. As differences in depth within the tissue were found to influence the observed fluorescence intensity for each cell, their mean values were normalized by setting the minimum and maximum fluorescence values to 0 and 10, respectively, while any value in between was approximated to an integer. This allowed us to define a fixed set of rules for easier peak identification from GCaMP6s mean fluorescence intensity data plotted against time. Peak durations were then estimated from the width of each peak at its base, and the comparison of the two sample types was performed in R with the Mann–Whitney two-tailed U test.

Ca^{2+} peak definitions for live-imaging experiments—Normalized GCaMP6s mean fluorescence intensity levels were plotted against time and used for peak identification. Original live-imaging data and maximum intensity projections were referenced to define the following rules and to randomly check the fidelity of the peaks identification. Fluorescence values 0 and 1 were defined as baseline, while 4 was set as the minimum value a peak has to reach to be defined as such. Peak starts were defined by a steady increase in fluorescence intensity from a baseline value. Alternatively, if a peak starts during the declining phase of a previous one, then the local minimum between the two peaks is set as the end of the first and the beginning of the second. Moreover, in order to be clearly visible when separating two distinct peaks, such local minimum must have a fluorescence value at least 3 points below the maximum point reached by the first peak. Lastly, peak ends were set as the lowest point reached during the declining phase of a peak (*e.g.*, either a baseline value or a local minimum). Since each time-point represents a 10” interval, peak durations were calculated as the difference between the time-points marking each peak’s end and start.

Bioinformatics analysis of cancer patient data—Mutation profile datasets for all human cancer studies used in this research were queried using the cBio Cancer Genomics Portal (cBioPortal version 2.0.1; accessed February 15, 2019). Genomic (whole exome sequencing) and clinicopathologic datasets of 619 colorectal adenocarcinoma samples (DFCI) (Giannakis et al., 2016) from The Cancer Genome Atlas (TCGA) (Cerami et al., 2012; Gao et al., 2013) were downloaded from cBioPortal. Differences in clinicopathologic characteristics (*e.g.*, microsatellite instability, CIMP status, *KRAS*) by mutation status were examined by chi-square tests. Analyses of TCGA data were conducted in SAS version 9.4 statistical software (SAS Institute; Cary, NC). All statistical tests were two-sided, with $P<0.05$ considered to be statistically significant.

Statistical analysis—Statistical analyses were performed using the Graphpad Prism 7 software package. Statistical significance (P values) of experiments were calculated by unpaired two-tailed Student's *t*-test. Statistical significance was denoted as follows: non-significant (ns) $P>0.05$, *$P<0.05$, **$P<0.01$, ***$P<0.001$ and ****$P<0.0001$.

Supplementary Material

Refer to Web version on PubMed Central for supplementary material.

ACKNOWLEDGEMENTS

We thank X. Lin, H. Knævelsrud, A. Rodal, D. Strutt, U. Banerjee, N. Perrimon, H. Jasper, J. Dixon, and X. Yang for fly stocks and antibodies. This work was supported by the Huntsman Cancer Foundation (to B.A.E. and C.M.U.) and grants from the National Institutes of Health (NIH: R01 GM124434 to B.A.E.; P30 CA042014 to B.A.E. and C.M.U.; U01 CA206110, R01 CA189184, and R01 CA211705 to C.M.U.). A.N.H. was supported by the NIH/National Human Genome Research Institute (T32 HG008962).

REFERENCES

Ahmed D, Eide PW, Eilertsen IA, Danielsen SA, Eknaes M, Hektoen M, Lind GE, and Lothe RA (2013). Epigenetic and genetic features of 24 colon cancer cell lines. Oncogenesis 2, e71. [PubMed: 24042735]

Antonacopoulou AG, Tsamandas AC, Petsas T, Liava A, Scopa CD, Papavassiliou AG, and Kalofonos HP (2008). EGFR, HER-2 and COX-2 levels in colorectal cancer. Histopathology 53, 698–706. [PubMed: 19102009]

Asano J, Sato T, Ichinose S, Kajita M, Onai N, Shimizu S, and Ohteki T (2017). Intrinsic Autophagy Is Required for the Maintenance of Intestinal Stem Cells and for Irradiation-Induced Intestinal Regeneration. Cell Rep 20, 1050–1060. [PubMed: 28768191]

Bardin AJ, Perdigoto CN, Southall TD, Brand AH, and Schweisguth F (2010). Transcriptional control of stem cell maintenance in the Drosophila intestine. Development 137, 705–714. [PubMed: 20147375]

Bel S, Pendse M, Wang Y, Li Y, Ruhn KA, Hassell B, Leal T, Winter SE, Xavier RJ, and Hooper LV (2017). Paneth cells secrete lysozyme via secretory autophagy during bacterial infection of the intestine. Science 357, 1047–1052. [PubMed: 28751470]

Buchon N, Broderick NA, Kuraishi T, and Lemaitre B (2010). Drosophila EGFR pathway coordinates stem cell proliferation and gut remodeling following infection. BMC Biol 8, 152. [PubMed: 21176204]

Cadwell K, Liu JY, Brown SL, Miyoshi H, Loh J, Lennerz JK, Kishi C, Kc W, Carrero JA, Hunt S, et al. (2008). A key role for autophagy and the autophagy gene Atg16l1 in mouse and human intestinal Paneth cells. Nature 456, 259–263. [PubMed: 18849966]

Cerami E, Gao J, Dogrusoz U, Gross BE, Sumer SO, Aksoy BA, Jacobsen A, Byrne CJ, Heuer ML, Larsson E, et al. (2012). The cBio cancer genomics portal: an open platform for exploring multidimensional cancer genomics data. Cancer Discov 2, 401–404. [PubMed: 22588877]

Ceresa BP (2006). Regulation of EGFR endocytic trafficking by rab proteins. Histol Histopathol 21, 987–993. [PubMed: 16763949]

Chang TK, Shravage BV, Hayes SD, Powers CM, Simin RT, Wade Harper J, and Baehrecke EH (2013). Uba1 functions in Atg7- and Atg3-independent autophagy. Nat Cell Biol 15, 1067–1078. [PubMed: 23873149]

Choi EJ, Lee JH, Kim MS, Song SY, Yoo NJ, and Lee SH (2017). Intratumoral Heterogeneity of Somatic Mutations for NRIP1, DOK1, ULK1, ULK2, DLGAP3, PARD3 and PRKCI in Colon Cancers. Pathol Oncol Res.

Choi JH, Hong WP, Kim MJ, Kim JH, Ryu SH, and Suh PG (2004). Sorting nexin 16 regulates EGF receptor trafficking by phosphatidylinositol-3-phosphate interaction with the Phox domain. J Cell Sci 117, 4209–4218. [PubMed: 15292396]

Cullen PJ (2008). Endosomal sorting and signalling: an emerging role for sorting nexins. Nat Rev Mol Cell Biol 9, 574–582. [PubMed: 18523436]

Cullis DN, Philip B, Baleja JD, and Feig LA (2002). Rab11-FIP2, an adaptor protein connecting cellular components involved in internalization and recycling of epidermal growth factor receptors. J Biol Chem 277, 49158–49166. [PubMed: 12364336]

Deng H, Gerencser AA, and Jasper H (2015). Signal integration by Ca(2+) regulates intestinal stem-cell activity. Nature 528, 212–217. [PubMed: 26633624]

Deniaud A, Sharaf el dein O, Maillier E, Poncet D, Kroemer G, Lemaire C, and Brenner C (2008). Endoplasmic reticulum stress induces calcium-dependent permeability transition, mitochondrial outer membrane permeabilization and apoptosis. Oncogene 27, 285–299. [PubMed: 17700538]

Edgar BA, and O'Farrell PH (1989). Genetic control of cell division patterns in the Drosophila embryo. Cell 57, 177–187. [PubMed: 2702688]

Ganley IG, Wong PM, Gammoh N, and Jiang X (2011). Distinct autophagosomal-lysosomal fusion mechanism revealed by thapsigargin-induced autophagy arrest. Mol Cell 42, 731–743. [PubMed: 21700220]

Gao J, Aksoy BA, Dogrusoz U, Dresdner G, Gross B, Sumer SO, Sun Y, Jacobsen A, Sinha R, Larsson E, et al. (2013). Integrative analysis of complex cancer genomics and clinical profiles using the cBioPortal. Sci Signal 6, pl1. [PubMed: 23550210]

Giannakis M, Mu XJ, Shukla SA, Qian ZR, Cohen O, Nishihara R, Bahl S, Cao Y, Amin-Mansour A, Yamauchi M, et al. (2016). Genomic Correlates of Immune-Cell Infiltrates in Colorectal Carcinoma. Cell Rep 17, 1206. [PubMed: 27760322]

Gissen P, and Maher ER (2007). Cargos and genes: insights into vesicular transport from inherited human disease. J Med Genet 44, 545–555. [PubMed: 17526798]

Guichard A, Nizet V, and Bier E (2014). RAB11-mediated trafficking in host-pathogen interactions. Nat Rev Microbiol 12, 624–634. [PubMed: 25118884]

Hay JC (2007). Calcium: a fundamental regulator of intracellular membrane fusion? EMBO Rep 8, 236–240. [PubMed: 17330068]

Issa JP (2004). CpG island methylator phenotype in cancer. Nat Rev Cancer 4, 988–993. [PubMed: 15573120]

Jiang H, and Edgar BA (2011). Intestinal stem cells in the adult Drosophila midgut. Exp Cell Res 317, 2780–2788. [PubMed: 21856297]

Jiang H, Grenley MO, Bravo MJ, Blumhagen RZ, and Edgar BA (2011). EGFR/Ras/MAPK signaling mediates adult midgut epithelial homeostasis and regeneration in Drosophila. Cell Stem Cell 8, 84–95. [PubMed: 21167805]

Jiang H, Patel PH, Kohlmaier A, Grenley MO, McEwen DG, and Edgar BA (2009). Cytokine/Jak/Stat signaling mediates regeneration and homeostasis in the Drosophila midgut. Cell 137, 1343–1355. [PubMed: 19563763]

Jin Y, Ha N, Fores M, Xiang J, Glasser C, Maldera J, Jimenez G, and Edgar BA (2015). EGFR/Ras Signaling Controls Drosophila Intestinal Stem Cell Proliferation via Capicua-Regulated Genes. PLoS Genet 11, e1005634. [PubMed: 26683696]

Jonker DJ, O'Callaghan CJ, Karapetis CS, Zalcberg JR, Tu D, Au HJ, Berry SR, Krahn M, Price T, Simes RJ, et al. (2007). Cetuximab for the treatment of colorectal cancer. N Engl J Med 357, 2040–2048. [PubMed: 18003960]

Kang MR, Kim MS, Oh JE, Kim YR, Song SY, Kim SS, Ahn CH, Yoo NJ, and Lee SH (2009). Frameshift mutations of autophagy-related genes ATG2B, ATG5, ATG9B and ATG12 in gastric and colorectal cancers with microsatellite instability. J Pathol 217, 702–706. [PubMed: 19197948]

Kitamoto T (2001). Conditional modification of behavior in Drosophila by targeted expression of a temperature-sensitive shibire allele in defined neurons. J Neurobiol 47, 81–92. [PubMed: 11291099]

Knaevelsrud H, Soreng K, Raiborg C, Haberg K, Rasmuson F, Brech A, Liestol K, Rusten TE, Stenmark H, Neufeld TP, et al. (2013). Membrane remodeling by the PX-BAR protein SNX18 promotes autophagosome formation. J Cell Biol 202, 331–349. [PubMed: 23878278]

Kondo Y, Kanzawa T, Sawaya R, and Kondo S (2005). The role of autophagy in cancer development and response to therapy. Nat Rev Cancer 5, 726–734. [PubMed: 16148885]

Kurten RC, Cadena DL, and Gill GN (1996). Enhanced degradation of EGF receptors by a sorting nexin, SNX1. Science 272, 1008–1010. [PubMed: 8638121]

Levine B, and Kroemer G (2008). Autophagy in the pathogenesis of disease. Cell 132, 27–42. [PubMed: 18191218]

Levy J, Cacheux W, Bara MA, L'Hermitte A, Lepage P, Fraudeau M, Trentesaux C, Lemarchand J, Durand A, Crain AM, et al. (2015). Intestinal inhibition of Atg7 prevents tumour initiation through a microbiome-influenced immune response and suppresses tumour growth. Nat Cell Biol 17, 1062–1073. [PubMed: 26214133]

Liang J, Balachandra S, Ngo S, and O'Brien LE (2017). Feedback regulation of steady-state epithelial turnover and organ size. Nature 548, 588–591. [PubMed: 28847000]

Lin Q, Lo CG, Cerione RA, and Yang W (2002). The Cdc42 target ACK2 interacts with sorting nexin 9 (SH3PX1) to regulate epidermal growth factor receptor degradation. J Biol Chem 277, 10134–10138. [PubMed: 11799118]

Matsuzawa-Ishimoto Y, Shono Y, Gomez LE, Hubbard-Lucey VM, Cammer M, Neil J, Dewan MZ, Lieberman SR, Lazrak A, Marinis JM, et al. (2017). Autophagy protein ATG16L1 prevents necroptosis in the intestinal epithelium. J Exp Med 214, 3687–3705. [PubMed: 29089374]

Micchelli CA, and Perrimon N (2006). Evidence that stem cells reside in the adult Drosophila midgut epithelium. Nature 439, 475–479. [PubMed: 16340959]

Miguel-Aliaga I, Jasper H, and Lemaitre B (2018). Anatomy and Physiology of the Digestive Tract of Drosophila melanogaster. Genetics 210, 357–396. [PubMed: 30287514]

Mulakkal NC, Nagy P, Takats S, Tusco R, Juhasz G, and Nezis IP (2014). Autophagy in Drosophila: from historical studies to current knowledge. Biomed Res Int 2014, 273473. [PubMed: 24949430]

Nagy P, Kovacs L, Sandor GO, and Juhasz G (2016). Stem-cell-specific endocytic degradation defects lead to intestinal dysplasia in Drosophila. Dis Model Mech 9, 501–512. [PubMed: 26921396]

Nagy P, Sandor GO, and Juhasz G (2018). Autophagy maintains stem cells and intestinal homeostasis in Drosophila. Sci Rep 8, 4644. [PubMed: 29545557]

Ogino S, and Goel A (2008). Molecular classification and correlates in colorectal cancer. J Mol Diagn 10, 13–27. [PubMed: 18165277]

Ohlstein B, and Spradling A (2006). The adult Drosophila posterior midgut is maintained by pluripotent stem cells. Nature 439, 470–474. [PubMed: 16340960]

Patel PH, Dutta D, and Edgar BA (2015). Niche appropriation by Drosophila intestinal stem cell tumours. Nat Cell Biol 17, 1182–1192. [PubMed: 26237646]

Pesic M, and Greten FR (2016). Inflammation and cancer: tissue regeneration gone awry. Curr Opin Cell Biol 43, 55–61. [PubMed: 27521599]

Pozzi C, Cuomo A, Spadoni I, Magni E, Silvola A, Conte A, Sigismund S, Ravenda PS, Bonaldi T, Zampino MG, et al. (2016). The EGFR-specific antibody cetuximab combined with chemotherapy triggers immunogenic cell death. Nat Med 22, 624–631. [PubMed: 27135741]

Rodal AA, Blunk AD, Akbergenova Y, Jorquera RA, Buhl LK, and Littleton JT (2011). A presynaptic endosomal trafficking pathway controls synaptic growth signaling. J Cell Biol 193, 201–217. [PubMed: 21464232]

Ryoo HD, Domingos PM, Kang MJ, and Steller H (2007). Unfolded protein response in a Drosophila model for retinal degeneration. EMBO J 26, 242–252. [PubMed: 17170705]

Senft D, and Ronai ZA (2015). UPR, autophagy, and mitochondria crosstalk underlies the ER stress response. Trends Biochem Sci 40, 141–148. [PubMed: 25656104]

Shaw RL, Kohlmaier A, Polesello C, Veelken C, Edgar BA, and Tapon N (2010). The Hippo pathway regulates intestinal stem cell proliferation during Drosophila adult midgut regeneration. Development 137, 4147–4158. [PubMed: 21068063]

Shukla S, Patric IR, Patil V, Shwetha SD, Hegde AS, Chandramouli BA, Arivazhagan A, Santosh V, and Somasundaram K (2014). Methylation silencing of ULK2, an autophagy gene, is essential for astrocyte transformation and tumor growth. J Biol Chem 289, 22306–22318. [PubMed: 24923441]

Sigismund S, Argenzio E, Tosoni D, Cavallaro E, Polo S, and Di Fiore PP (2008). Clathrin-mediated internalization is essential for sustained EGFR signaling but dispensable for degradation. Dev Cell 15, 209–219. [PubMed: 18694561]

Singh SR, Zeng X, Zhao J, Liu Y, Hou G, Liu H, and Hou SX (2016). The lipolysis pathway sustains normal and transformed stem cells in adult Drosophila. Nature 538, 109–113. [PubMed: 27680705]

Sorkin A, and Von Zastrow M (2002). Signal transduction and endocytosis: close encounters of many kinds. Nat Rev Mol Cell Biol 3, 600–614. [PubMed: 12154371]

Spalluto C, Wilson DI, and Hearn T (2013). Evidence for reciliation of RPE1 cells in late G1 phase, and ciliary localisation of cyclin B1. FEBS Open Bio 3, 334–340.

Strutt H, Warrington SJ, and Strutt D (2011). Dynamics of core planar polarity protein turnover and stable assembly into discrete membrane subdomains. Dev Cell 20, 511–525. [PubMed: 21497763]

Takats S, Nagy P, Varga A, Pircs K, Karpati M, Varga K, Kovacs AL, Hegedus K, and Juhasz G (2013). Autophagosomal Syntaxin17-dependent lysosomal degradation maintains neuronal function in Drosophila. J Cell Biol 201, 531–539. [PubMed: 23671310]

Tang HW, Liao HM, Peng WH, Lin HR, Chen CH, and Chen GC (2013). Atg9 interacts with dTRAF2/TRAF6 to regulate oxidative stress-induced JNK activation and autophagy induction. Dev Cell 27, 489–503. [PubMed: 24268699]

Teasdale RD, and Collins BM (2012). Insights into the PX (phox-homology) domain and SNX (sorting nexin) protein families: structures, functions and roles in disease. Biochem J 441, 39–59. [PubMed: 22168438]

Tooze SA, Abada A, and Elazar Z (2014). Endocytosis and autophagy: exploitation or cooperation? Cold Spring Harb Perspect Biol 6, a018358. [PubMed: 24789822]

Toyota M, Ahuja N, Ohe-Toyota M, Herman JG, Baylin SB, and Issa JP (1999). CpG island methylator phenotype in colorectal cancer. Proc Natl Acad Sci U S A 96, 8681–8686. [PubMed: 10411935]

Vessoni AT, Muotri AR, and Okamoto OK (2012). Autophagy in stem cell maintenance and differentiation. Stem Cells Dev 21, 513–520. [PubMed: 22066548]

Vieira AV, Lamaze C, and Schmid SL (1996). Control of EGF receptor signaling by clathrin-mediated endocytosis. Science 274, 2086–2089. [PubMed: 8953040]

Vilar E, and Gruber SB (2010). Microsatellite instability in colorectal cancer-the stable evidence. Nat Rev Clin Oncol 7, 153–162. [PubMed: 20142816]

Vodovar N, Vinals M, Liehl P, Basset A, Degrouard J, Spellman P, Boccard F, and Lemaitre B (2005). Drosophila host defense after oral infection by an entomopathogenic Pseudomonas species. Proc Natl Acad Sci U S A 102, 11414–11419. [PubMed: 16061818]

Weisenberger DJ, Siegmund KD, Campan M, Young J, Long TI, Faasse MA, Kang GH, Widschwendter M, Weener D, Buchanan D, et al. (2006). CpG island methylator phenotype underlies sporadic microsatellite instability and is tightly associated with BRAF mutation in colorectal cancer. Nat Genet 38, 787–793. [PubMed: 16804544]

Wen JK, Wang YT, Chan CC, Hsieh CW, Liao HM, Hung CC, and Chen GC (2017). Atg9 antagonizes TOR signaling to regulate intestinal cell growth and epithelial homeostasis in Drosophila. Elife 6.

White E, and DiPaola RS (2009). The double-edged sword of autophagy modulation in cancer. Clin Cancer Res 15, 5308–5316. [PubMed: 19706824]

Worby CA, Simonson-Leff N, Clemens JC, Kruger RP, Muda M, and Dixon JE (2001). The sorting nexin, DSH3PX1, connects the axonal guidance receptor, Dscam, to the actin cytoskeleton. J Biol Chem 276, 41782–41789. [PubMed: 11546816]

Xiang J, Bandura J, Zhang P, Jin Y, Reuter H, and Edgar BA (2017). EGFR-dependent TOR-independent endocycles support Drosophila gut epithelial regeneration. Nat Commun 8, 15125. [PubMed: 28485389]

Xu C, Luo J, He L, Montell C, and Perrimon N (2017). Oxidative stress induces stem cell proliferation via TRPA1/RyR-mediated Ca(2+) signaling in the Drosophila midgut. Elife 6.

Zeng X, Han L, Singh SR, Liu H, Neumuller RA, Yan D, Hu Y, Liu Y, Liu W, Lin X, et al. (2015). Genome-wide RNAi screen identifies networks involved in intestinal stem cell regulation in Drosophila. Cell Rep 10, 1226–1238. [PubMed: 25704823]

Zhang P, Wu Y, Belenkaya TY, and Lin X (2011). SNX3 controls Wingless/Wnt secretion through regulating retromer-dependent recycling of Wntless. Cell Res 21, 1677–1690. [PubMed: 22041890]

Highlights

- Ectoderm-derived metaphocytes in zebrafish epidermis are myeloid-like cells
- Unlike Langerhans cells, highly mobile metaphocytes lack phagocytosis ability
- Metaphocytes capture external soluble antigens through transepithelial protrusions
- Antigen transfer from metaphocytes to Langerhans cells via apoptosis-phagocytosis

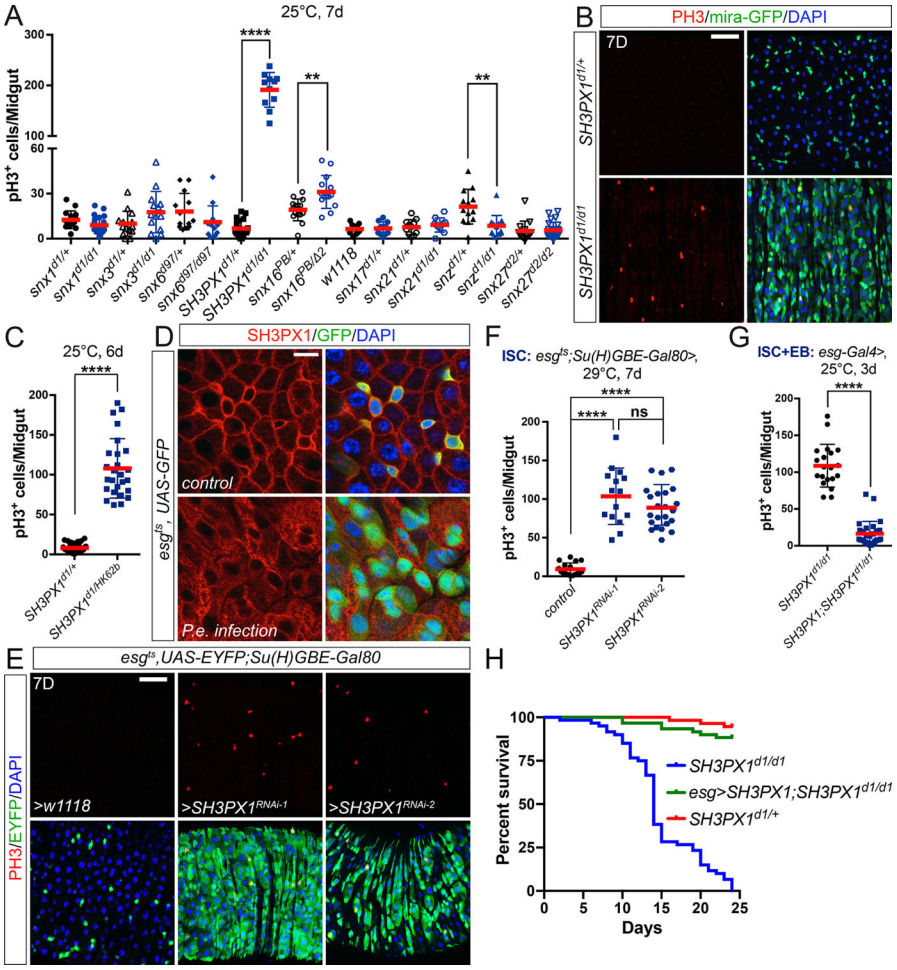

Figure 1. *Drosophila* SH3PX1 restrains ISC proliferation

(A, C, F, G) Midguts were stained with anti-pH3 antibody. ISC mitoses were quantified by pH3^{+} cells. Quantification data shown in A, C, F, and G represent the mean±SD (*t*-test, ^{ns}P>0.05, **P<0.01, ****P<0.0001). Each dot represents one sample. (B, E) Midguts were stained with anti-GFP and anti-pH3 antibodies, and DAPI. (D) 2–3 day-old *esg-Gal4,UAS-GFP;tubGal80^{ts}* (*esg^{ts}*) flies were shifted from 18°C to 29°C and raised for 2d on normal fly food before infection. Flies were then transferred to empty vials containing Whatman discs soaked with 5% sucrose and yeast paste +/− *P.e.* for 16hr at 29°C. Midguts were dissected and stained with anti-SH3PX1 antibody. (E-F) Two independent *RNAi* lines against *SH3PX1* were driven using an ISC-specific driver *esg-Gal4,UAS-2xEYFP;Su(H)GBE-Gal80,tub-Gal80^{ts}* (*esg^{ts};Su(H)GBE-Gal80*). 2–3 day-old adult females were shifted from 18°C to 29°C for 7d before dissection. The *SH3PX1^{RNAi}* lines' knockdown efficiencies are shown in Supplementary Figures 2A–2C'. (G) *UAS-GFP-SH3PX1* was overexpressed using *esg-Gal4* at 25°C for 3d in the *SH3PX1$^{d1/d1}$* mutant background. (H) Flies were raised at 25°C on normal fly food. Survival curves are shown for each genotype as indicated (n=30, per genotype). Scale bars in B and E, 40 μm; D, 10 μm.

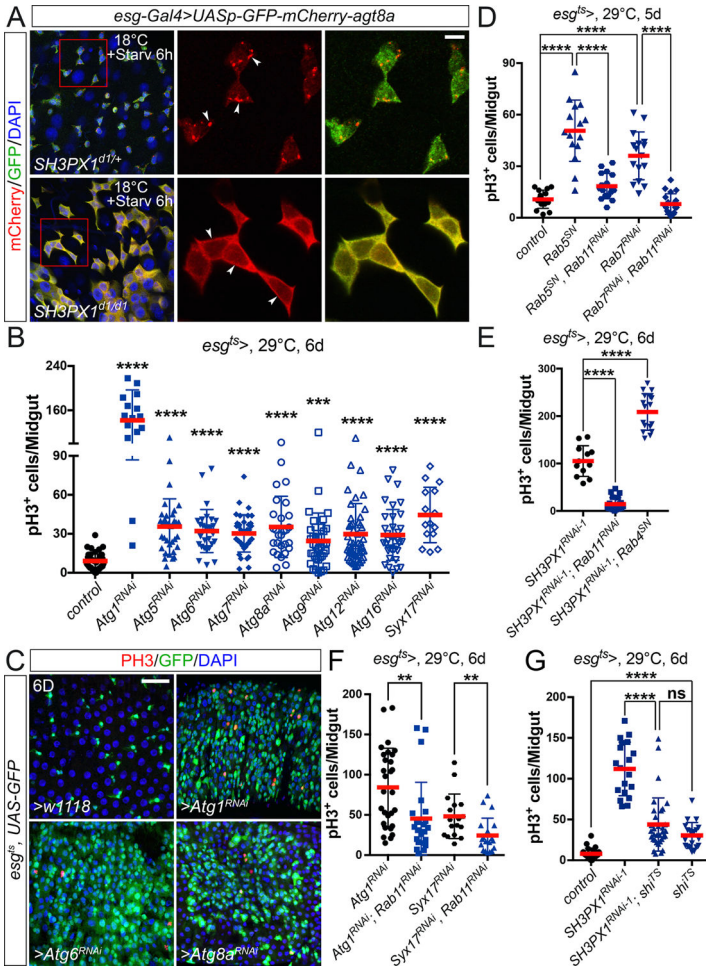

Figure 2. SH3PX1-dependent autophagy restricts ISC proliferation

(A) Flies were raised at 18°C. 3-day-old *esg-Gal4/UASp-GFP-mCherry-atg8a;SH3PX1^{d1}FRT^{2A}/TM6B* or *esg-Gal4/UASp-GFP-mCherry-atg8a;SH3PX1^{d1}FRT^{2A}/SH3PX1^{d1}FRT^{2A}* flies were starved for 6hr in the vials containing Whatman paper wetted with 5% sucrose, then were stained with anti-GFP and anti-RFP antibodies, and DAPI. *esgGal4>UASp-GFP-mCherry-atg8a* marked autophagosomes in progenitor cells. The red boxes in the left panels were enlarged and visualized in the middle/right panels. Arrowheads indicate autophagosome formation. (B-G) Different genetic manipulations in progenitor cells driven by *esg^{ts}*. 2~3-day-old adult females were shifted from 18°C to 29°C for 5–6d (as indicated in panels) before dissection. Midguts were stained with anti-GFP and anti-pH3 antibodies, and DAPI. ISC mitoses were quantified by pH3^{+} cells. Quantification data shown in B, D-G represent the mean±SD (*t*-test, ^{ns}P>0.05, **P<0.01, ***P<0.001, ****P<0.0001). Each dot represents one sample. Scale bars in A, 5 μm; C, 40 μm.

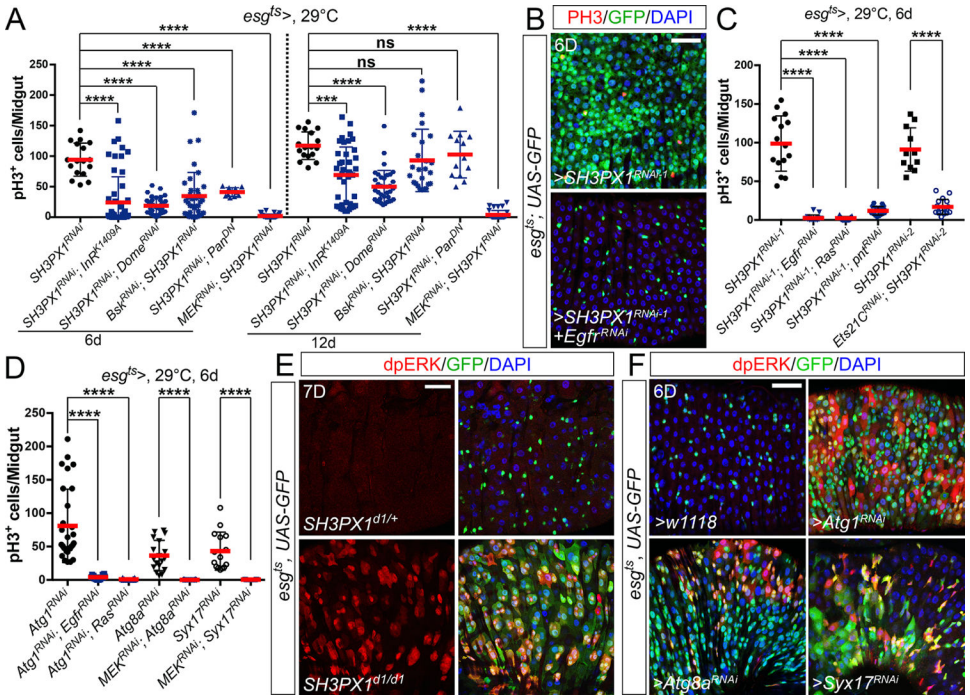

Figure 3. SH3PX1-mediated autophagy restrains ISC mitoses by damping EGFR/ERK activity

(A-D) Different genetic manipulations in progenitor cells driven by *esg*^{ts}. 2~3-day-old adult females were shifted from 18°C to 29°C for 6d or 12d (as indicated in panels) before dissection. Midguts were stained with anti-GFP and anti-pH3 antibodies, and DAPI. ISC mitoses were quantified by pH3^{+} cells. Quantification data shown in A, C and D represent the mean±SD (*t*-test, ^{ns}P>0.05, ****P<0.0001). Each dot represents one sample. (E-F) Flies with indicated genetic manipulations were shifted from 18°C to 29°C for 6d or 7d (as indicated in panels) before dissection. Midguts were stained with anti-GFP and anti-dpERK antibodies, and DAPI. Scale bars in B, E and F, 40 μm.

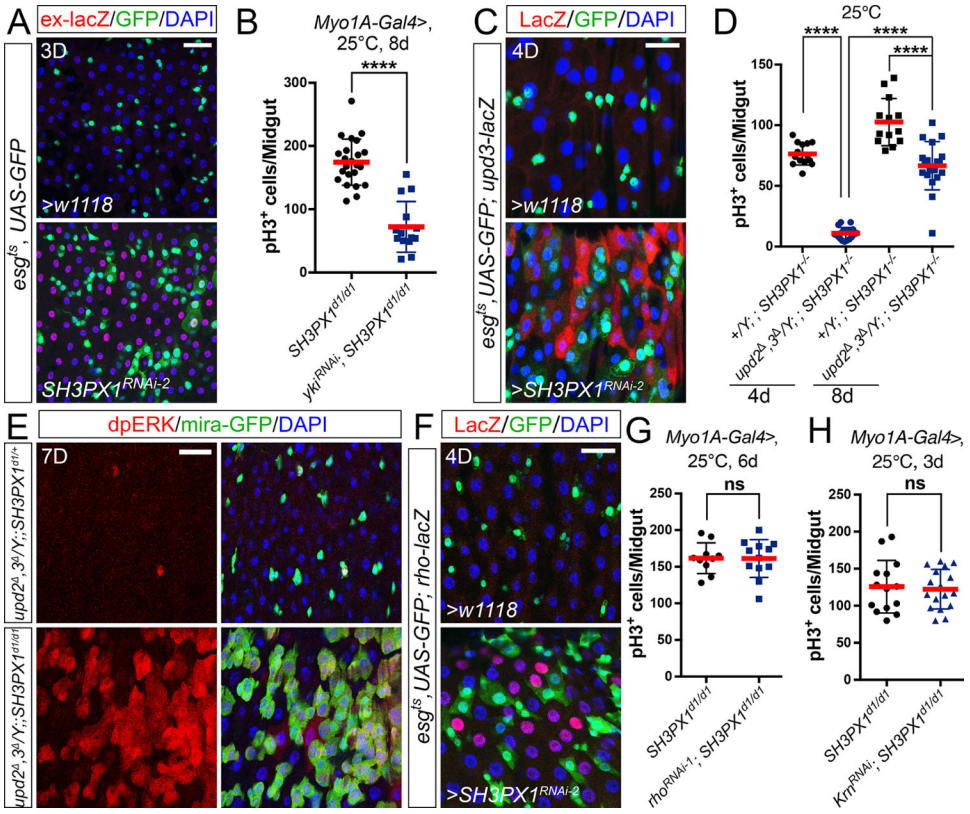

Figure 4. EC-localized stress signaling is dispensable for proliferation of *SH3PX1* mutant ISCs

(A, C, F) *UAS-SH3PX1*$^{RNAi-2}$ was overexpressed using *esg*^{ts} at 29°C for 3d or 4d, as indicated in panels before dissection. *Ex-lacZ* (A, red) expression indicated Yki activity. *Upd3* expression levels were indicated by the *upd3-lacZ* reporter (C, red). *Rho* induction was indicated by the *rho-lacZ* reporter (F, red). Progenitor cells were marked by GFP. (B, D, G and H) Midguts were stained with anti-pH3 antibody. ISC mitoses were quantified by pH3^{+} cells. (B) *UAS-yki*^{RNAi} was overexpressed using *myo1A-Gal4* at 25°C for 8d in the *SH3PX1*$^{d1/d1}$ mutant background. (D) Adult males of *+/Y;mira-GFP;SH3PX1*$^{d1/d1}$ (control) and *upd2*^{Δ},*3*^{Δ} */Y;mira-GFP;SH3PX1*$^{d1/d1}$ were incubated at 25°C for 4 or 8d after eclosion. (E) The same genotype flies as described in panel D were stained with anti-GFP and anti-dpERK antibodies and DAPI at day 7. (G-H) *UAS-rho*^{RNAi} (G) or *UAS-Krn*^{RNAi} (H) was overexpressed using *Myo1A-Gal4* at 25°C for 3d or 6d (as indicated in panels) in the *SH3PX1*$^{d1/d1}$ mutant background. Quantification data shown in C, D, G and H represent the mean±SD (*t*-test, ^{ns}P>0.05, ****P<0.0001). Each dot represents one sample. Scale bars in A, 30 μm; C, E and F, 20 μm.

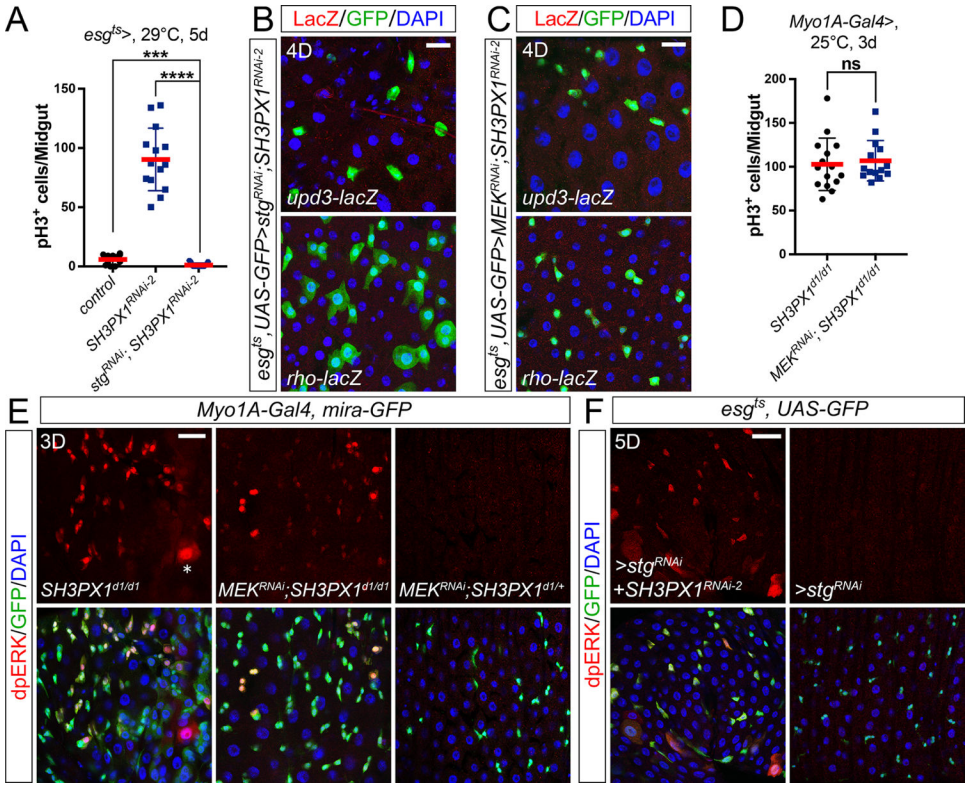

Figure 5. Cell autonomous EGFR/MAPK activation triggers *SH3PX1*⁻-ISC division

(A, D) Midguts were stained with anti-pH3 antibody. ISC mitoses were quantified by pH3$^+$ cells. (A) *SH3PX1* knockdown or *SH3PX1/stg* double knockdown was driven by *esg^{ts}*. *esg^{ts}>w1118* was used as control. Flies were raised at 18°C and then shifted to 29°C for 5d before dissection. (B-C) *SH3PX1/stg* or *SH3PX1/MEK* double knockdown was driven by *esg^{ts}* at 29°C for 4d. Induction of *upd3* or *rho* was indicated by *upd3-lacZ* (upper panels of B, and C) or *rho-lacZ* (lower panels of B, and C), respectively. Progenitor cells were marked by GFP. (D-E) *UAS-MEK^{RNAi}* was overexpressed using *myo1A-Gal4* at 25°C for 3d in the *SH3PX1$^{d1/d1}$* mutant background. *Myo1A-Gal4/+;SH3PX1$^{d1/d1}$* flies were selected as positive control (D and left panels of E). *Myo1A-Gal4/MEK^{RNAi}; SH3PX1$^{d1/+}$* flies were selected as negative control (E, right panels). (E-F) Midguts were stained with anti-GFP antibody and anti-dpERK antibodies, and DAPI. White asterisk in (E) indicates the EC cell. (F) *SH3PX1* knockdown (control) or *SH3PX1/stg* double knockdown was driven by *esg^{ts}* at 29°C for 5d. Quantification data shown in A and D represent the mean ± SD (*t*-test, nsP>0.05, ***P<0.001, ****P<0.0001). Each dot represents one sample. Scale bars in B and C, 20 μm; E, 30 μm; F, 40 μm.

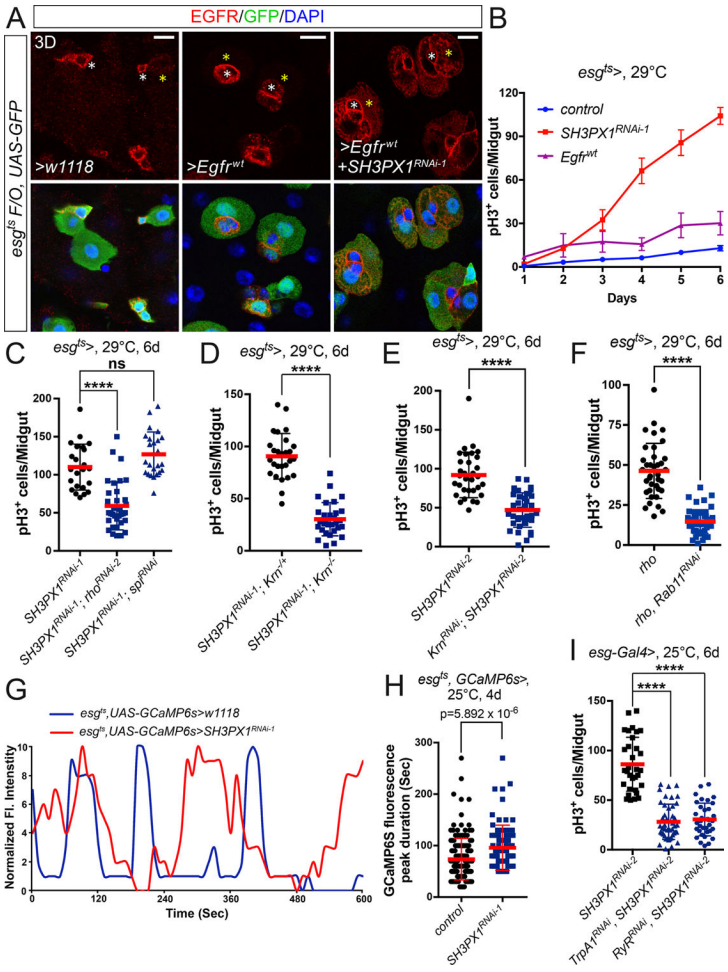

Figure 6. SH3PX1 controls the EGFR pathway via multiple routes

(A) *UAS-EGFR*^{wt} or *UAS-SH3PX1*$^{RNAi-1}$*+UAS-EGFR*^{wt} was overexpressed by the *esg*^{ts}*F/O* system. *Esg*^{ts}*F/O>w1118* was used as control. Flies were raised at 18°C and then shifted to 29°C for 3d before dissection. Midguts were stained with anti-EGFR and anti-GFP antibodies, and DAPI. White asterisks indicate ISC or EB cells. Yellow asterisks indicate EC cells. (B) *w1118*, *UAS-SH3PX1*$^{RNAi-1}$ and *UAS-EGFR*^{wt} were overexpressed by *esg*^{ts}. Flies were raised at 18°C and then shifted to 29°C for 1–6d before dissection. Samples were dissected every day from d1 to d6 and stained with anti-pH3 antibody. ISC mitoses were quantified by pH3^{+} cells. Values represent mean±SEM. (C-F, I) Midguts were stained with anti-pH3 antibody. ISC mitoses were quantified by pH3^{+} cells. (C-F) Different genetic manipulations in progenitor cells driven by *esg*^{ts}. 2~3-day-old adult females were shifted from 18°C to 29°C for 6d before dissection. (G-H) *UAS-GCaMP6s* or together with *UAS-SH3PX1*$^{RNAi-1}$ was overexpressed using *esg*^{ts}. (G) Representative Ca^{2+} plots of single *esg*$^{+}$ midgut cells from wild-type (blue) and *SH3PX1* knockdown (red) flies. Normalized fluorescence intensity is plotted over time, highlighting differences in intracellular Ca^{2+} peak durations. (H) Peak durations as determined from Ca^{2+} plots of wild-type (n=155 peaks) and *SH3PX1* knockdown (n=80 peaks) *esg*$^{+}$ midgut cells; P-value calculated by Mann-Whitney two-tailed U test. (I) *SH3PX1* knockdown, *SH3PX1/TrpA1* double knockdown, and *SH3PX1/RyR* double knockdown were driven by *esg-Gal4* at 25°C for 6d.

Quantification data shown in C-F and I represent the mean±SD (*t*-test, ^{ns}P>0.05, ****P<0.0001). Each dot represents one sample. Scale bars in A, 10 μm.

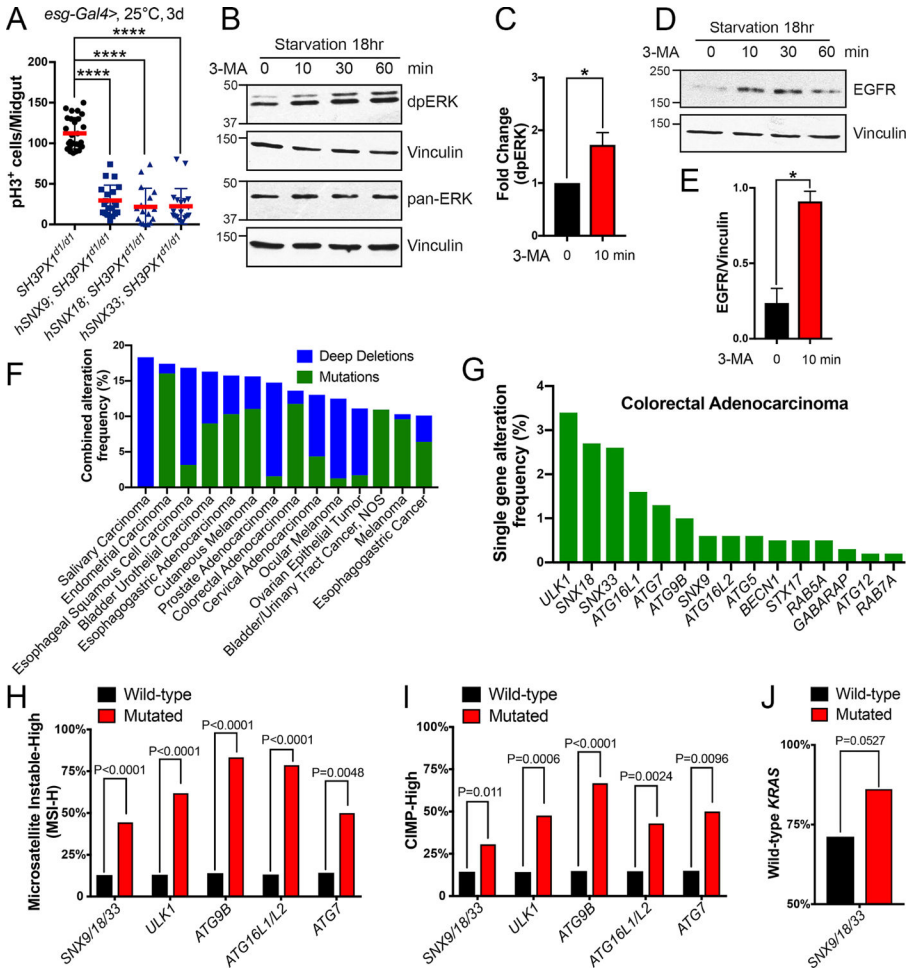

Figure 7. Autophagy mutations are associated with MSI-H and CIMP-H colorectal cancers

(A) *UAS-hSNX9, hSNX18 or hSNX33* were overexpressed using *esg-Gal4* at 25°C for 3d in the *SH3PX1*$^{d1/d1}$ mutant background. (B-E) RPE-1 cells were serum starved for 18hr, then treated with the autophagy inhibitor, 3-MA (4mM), for the times indicated. Cell lysates were subjected to western blot analysis with the indicated antibodies. (C) The induction (fold change) of dpERK samples in (B) was quantified after normalization against total-ERK. Values represent mean±SEM (n=4 independent experiments, *t*-test, *P<0.05). (E) The relative levels of EGFR shown in (D) were quantified after normalization against Vinculin. Values represent mean±SEM (n=2 independent experiments, *t*-test, *P<0.05). (F) Summary of SH3PX1-dependent endocytosis/autophagy mutations and deep deletions by cancer type in human TCGA datasets (n=14 datasets with ≥10% mutation and deep deletion alteration frequency and n³30 cases). The network gene list and corresponding human orthologs are shown in Table S1. (G-J) Analysis of somatic mutations in human colorectal adenocarcinoma (DFCI, n=619 cases). (G) Summary of somatic mutations by gene. (H-J) Proportion of wild-type (black) versus mutated (red) samples with the MSI-H genomic phenotype (H) and the CIMP-H epigenomic phenotype (I) (n=5 genes with ≥1% altered cases). (J) Proportion of *SH3PX1* human homologs *SNX9/18/33* wild-type versus mutated samples by *KRAS* wild-type status.

KEY RESOURCES TABLE

REAGENT or RESOURCE	SOURCE	IDENTIFIER
Antibodies		
Chicken α-GFP	Thermo Fisher Scientific	Cat# A10262; RRID: AB_2534023
Rabbit α-DsRed	Clontech Laboratories, Inc.	Cat# 632496; RRID: AB_10013483
Rabbit α-phospho-Histone 3	Millipore	Cat# 06–570; RRID: AB_310177
Mouse α-phospho-Histone 3	Cell Signaling Technology	Cat# 9706; RRID: AB_331748
Rabbit α-phospho-p44/42 MAPK (Erk1/2)	Cell Signaling Technology	Cat# 4370; RRID: AB_2315112
Mouse α-p44/42 MAPK (Erk1/2)	Cell Signaling Technology	Cat# 9107; RRID: AB_10695739
Mouse α-β-galactosidase	Promega	Cat# Z3781; RRID: AB_430877
Mouse α-dEGFR	Sigma-Aldrich	Cat# E2906; RRID: AB_609900
Rabbit α-EGFR	Cell Signaling Technology	Cat# 4267; RRID: AB_2246311
Rabbit α-SH3PX1	Jack Dixon (UCSD, USA)	N/A
Mouse α-Prospero	DHSB	Cat# Prospero (MR1A); RRID: AB_528440
Rabbit α-Pdm1	Xiaohang Yang (ZJU, China)	N/A
Mouse α-alpha-tubulin	DHSB	Cat# 12G10; RRID: AB_1157911
Mouse α-vinculin	Sigma-Aldrich	Cat# V9131; RRID: AB_477629
Bacterial and Virus Strains		
Pseudomonas entomophila (*P.e.*)	Nicolas Buchon (Cornell University)	N/A
Biological Samples		
N/A	N/A	N/A
Chemicals, Peptides, and Recombinant Proteins		
DAPI	Thermo Fisher Scientific	Cat# D1306; RRID: AB_2629482
Critical Commercial Assays		
N/A	N/A	N/A
Deposited Data		
N/A	N/A	N/A
Experimental Models: Cell Lines		
N/A	N/A	N/A
Experimental Models: Organisms/Strains		
Drosophila: snx1^{d1}	(Zhang et al., 2011)	CG2774
Drosophila: snx3^{d1}	(Zhang et al., 2011	CG6359

REAGENT or RESOURCE	SOURCE	IDENTIFIER
Drosophila: snx6^{d97}	(Zhang et al., 2011)	CG8282
Drosophila: SH3PX1^{d1}	(Zhang et al., 2011)	CG6757
Drosophila: SH3PX1^{HK62b}	(Knaevelsrud et al., 2013)	CG6757
Drosophila: snx16^{PB}	(Rodal et al., 2011)	CG6410
Drosophila: snx16^{A2}	(Rodal et al., 2011)	CG6410
Drosophila: snx17^{d1}	(Zhang et al., 2011)	CG5734
Drosophila: snx21^{d1}	(Zhang et al., 2011)	CG3077
Drosophila: snz^{d1}	(Zhang et al., 2011)	CG1514
Drosophila: snx27^{d2}	(Zhang et al., 2011)	CG32758
Drosophila: esg-Gal4, UAS-2xEYFP/CyO; Su(H)GBE-Gal80, tubGal80^{s}/TM3	Heinrich Jasper (Genentech)	N/A
Drosophila: esg-Gal4, UAS-GFP/CyO; tubGal80^{s}/TM6B	(Jiang et al., 2009)	N/A
Drosophila: esg-Gal4, UAS-GFP, tubGal80^{s}/CyO	Bruce A. Edgar (HCI, USA)	N/A
Drosophila: tubGal80^{s}/FM7; esg-Gal4/CyO	Bruce A. Edgar (HCI, USA)	N/A
Drosophila: Su(H)GBE-Gal4, UAS-GFP/CyO; Ubi-Gal80^{s}/TM6B	(Xiang et al., 2017)	N/A
Drosophila: Myo1A-Gal4, tubGal80^{s}, UAS-GFP/CyO	(Jiang et al., 2009)	N/A
Drosophila: tub-Gal80^{s}, UAS-GFP/CyO; prosV1-Gal4/TM6B	This paper	N/A
Drosophila: esg-Gal4, tub-Gal80^{s}, UAS-GFP/CyO; UAS-flp, act>CD2>Gal4/TM6B	(Jiang et al., 2009)	N/A
Drosophila: hs-flp; act-Gal4, UAS-mRFP; tub-Gal80 FRT^{2A}/TM6B	Bruce A. Edgar (HCI, USA)	N/A
Drosophila: hs-flp, UAS-GFP, act-Gal4; ; FRT^{2A} UAS-Gal80/TM6	Bruce A. Edgar (HCI, USA)	N/A
Drosophila: enGal4	(Zhang et al., 2017)	N/A
Drosophila: mira-GFP	(Bardin et al., 2010)	N/A
Drosophila: Myo1A-Gal4, mira-GFP/CyO; MKRS/TM6B	This paper	N/A
Drosophila: ex-lacZ	(Zhang et al., 2017)	N/A
Drosophila: upd3.1-lacZ	(Jiang et al., 2011)	N/A
Drosophila: rho-lacZ	(Jiang et al., 2011)	N/A
Drosophila: UASp-GFP-mCherry-atg8a	BDSC	37750
Drosophila: UAS-SH3PX1^{RNAi-1}	BDSC	54833
Drosophila: UAS-SH3PX1^{RNAi-2}	BDSC	27653
Drosophila: UAS-SH3PX1^{EY08084}	BDSC	17428
Drosophila: UAS-GFP-SH3PX1	Helene Knævelsrud (Oslo University Hospital)	N/A
Drosophila: UAS-Atg1^{RNAi}	VDRC	16133
Drosophila: UAS-Atg5^{RNAi}	BDSC	34899
Drosophila: UAS-Atg6^{RNAi}	BDSC	35741
Drosophila: UAS-Atg7^{RNAi}	BDSC	34369
Drosophila: UAS-Atg8a^{RNAi}	BDSC	34340

REAGENT or RESOURCE	SOURCE	IDENTIFIER
Drosophila: UAS-Atg9^{RNAi}	BDSC	34901
Drosophila: UAS-Atg12^{RNAi}	BDSC	34675
Drosophila: UAS-Atg16^{RNAi}	BDSC	34358
Drosophila: UAS-Syx17^{RNAi}	BDSC	25896
Drosophila: UAS-Rab4^{SN}	(Strutt et al., 2011)	N/A
Drosophila: UAS-Rab5^{SN}	(Strutt et al., 2011)	N/A
Drosophila: UAS-Rab7^{RNAi}	VDRC	40337
Drosophila: UAS-Rab11^{RNAi}	BDSC	27730
Drosophila: UAS-shi^{TS}	BDSC	44222
Drosophila: UAS-InR^{K1409A}	BDSC	8253
Drosophila: UAS-Dome^{RNAi}	BDSC	34618
Drosophila: UAS-Bsk^{RNAi}	VDRC	34138
Drosophila: UAS-Pan^{DN}	BDSC	4785
Drosophila: UAS-Egfr^{RNAi}	BDSC	25781
Drosophila: UAS-Ras^{RNAi}	BDSC	29319
Drosophila: UAS-MEK^{RNAi}	VDRC	107276
Drosophila: UAS-pnt^{RNAi}	Bruce A. Edgar (HCI, USA)	N/A
Drosophila: UAS-Ets21C^{RNAi}	VDRC	106153
Drosophila: UAS-Pvr^{RNAi}	Utpal Banerjee (UCLA, USA)	N/A
Drosophila: UAS-btl^{RNAi}	Bruce A. Edgar (HCI, USA)	N/A
Drosophila: UAS-upd3^{RNAi}	VDRC	106869
Drosophila: upd2$^{\Delta}$, upd3$^{\Delta}$	BDSC	55729
Drosophila: UAS-rho^{RNAi-1}	BDSC	41699
Drosophila: UAS-rho^{RNAi-2}	BDSC	28690
Drosophila: UAS-Krn^{RNAi}	NIG	8056R-3
Drosophila: Krn^{27-7-4}	(Jiang et al., 2011)	N/A
Drosophila: UAS-spi^{RNAi}	BDSC	28387
Drosophila: UAS-stg^{RNAi}	NIG	1395R-1
Drosophila: UAS-Egfr^{wt}	(Xiang et al., 2017)	N/A
Drosophila: UAS-xbp1-EGFP	BDSC	39720
Drosophila: UAS-GCaMP6s	BDSC	42749
Drosophila: UAS-TrpA1^{RNAi}	BDSC	31504
Drosophila: UAS-RyR^{RNAi}	BDSC	29445
Drosophila: UAS-V5-hSNX9	This paper	N/A
Drosophila: UAS-V5-hSNX18	This paper	N/A
Drosophila: UAS-V5-hSNX33	This paper	N/A
Oligonucleotides		
N/A	N/A	N/A

REAGENT or RESOURCE	SOURCE	IDENTIFIER
Recombinant DNA		
cDNA: Human SNX9	GenScript USA Inc.	Clone ID: OHu12143; RefSeq Accession: NM_016224.4
cDNA: Human SNX18	GenScript USA Inc.	Clone ID: OHu08909; RefSeq Accession: NM_052870.2
cDNA: Human SNX33	GenScript USA Inc.	Clone ID: OHu30854; RefSeq Accession: NM_153271.1
Plasmid: pUASTattB-V5-hSNX9	This paper	N/A
Plasmid: pUASTattB-V5-hSNX18	This paper	N/A
Plasmid: pUASTattB-V5-hSNX33	This paper	N/A
Software and Algorithms		
Prism 7	GraphPad Software	RRID: SCR_002798
ImageJ	https://fiji.sc	N/A
R package	https://www.r-project.org	N/A
SAS version 9.4 statistical software	SAS Institute; Cary, NC	N/A
cBioPortal	http://www.cbioportal.org	N/A
The Cancer Genome Atlas (TCGA)	https://cancergenome.nih.gov	N/A
Other		
N/A	N/A	N/A